AGU PUBLICATIONS

JGR

Journal of Geophysical Research: Oceans

RESEARCH ARTICLE

10.1002/2015JC010879

On the dynamics of the Zanzibar Channel

J. Zavala-Garay[1], J. Theiss[2], M. Moulton[3], C. Walsh[4], R. van Woesik[5], C. G. Mayorga-Adame[6], M. García-Reyes[7], D. S. Mukaka[8], K. Whilden[9], and Y. W. Shaghude[8]

[1]Ocean Modeling Group, Institute of Marine and Coastal Sciences, Rutgers, New Jersey, USA, [2]Theiss Research, La Jolla, California, USA, [3]Department of Applied Ocean Physics and Engineering, Woods Hole Oceanographic Institution, Woods Hole, Massachusetts, USA, [4]Electrical and Computer Engineering, Carnegie Mellon University, Pittsburgh, Pennsylvania, USA, [5]Harris Center For Science and Engineering, Florida Institute of Technology, Melbourne, Florida, USA, [6]College of Ocean, Earth, and Atmospheric Sciences, Oregon State University, Corvallis, Oregon, USA, [7]Farallon Institute for Advanced Ecosystem Research, Petaluma, California, USA, [8]Institute of Marine Sciences, University of Dar es Salaam, Zanzibar, Tanzania, [9]Zachry Department of Civil Engineering, Texas A&M University, College Station, Texas, USA

Key Points:
- Seasonal dynamics of the Zanzibar Channel forced remotely and by local wind
- Tides converge and diverge in the center of the channel and reduce the transport
- 5%, 3%, and 92% of kinetic energy in remotely, wind, and tidal-forced dynamics

Correspondence to:
J. Zavala-Garay,
jzavala@marine.rutgers.edu

Citation:
Zavala-Garay, J., J. Theiss, M. Moulton, C. Walsh, R. Woesik, C. G. Mayorga-Adame, M. García-Reyes, D. S. Mukaka, K. Whilden, and Y. W. Shaghude (2015), On the dynamics of the Zanzibar Channel, *J. Geophys. Res. Oceans*, *120*, 6091–6113, doi:10.1002/2015JC010879.

Received 27 MAR 2015
Accepted 22 JUL 2015
Accepted article online 24 JUL 2015
Published online 12 SEP 2015

Abstract The Zanzibar Channel lies between the mainland of Tanzania and Zanzibar Island in the tropical western Indian Ocean, is about 100 km long, 40 km wide, and 40 m deep, and is essential to local socioeconomic activities. This paper presents a model of the seasonal and tidal dynamics of the Zanzibar Channel based on the Regional Ocean Modeling System (ROMS) and a comparison of the model and observations. The seasonal dynamics of the channel is forced by remote processes and the local wind. Remote forcing creates the East African Coastal Current, a portion of which flows through the channel northward with a seasonally varying magnitude. The local wind enhances this seasonality in the surface Ekman layer, resulting in a stronger northward flow during the southwest monsoon season and a weak northward or occasionally southward flow during the northeast monsoon season. The tidal flows converge and diverge in the center of the channel and reduce the transport in the channel. The remotely forced, wind-forced, and tidal dynamics contain 5%, 3%, and 92% of the total kinetic energy, respectively. Despite their low kinetic energy, the remotely forced and wind-forced flows are most relevant in advecting channel water to the open ocean, which occurs in 19 days at the peak of the southwest monsoon season. The channel is well mixed, except during brief periods in the two rainy seasons, and temporarily cools between December and February. The dispersion of passive tracers is presented as an example of potential model applications.

1. Introduction

Healthy coastal and marine resources are essential for fisheries, tourism, offshore mining, and other socioeconomic activities. These resources face increasing threats associated with the growth of coastal populations, the impacts of natural hazards, e.g., storm surge and flooding, in increasingly developed areas, and the effects of climate change, e.g., sea level rise and coral bleaching [*Odido and Mazzilli*, 2009]. Sustainable management of coastal and marine resources is therefore paramount. However, many developing countries lack the appropriate tools to make science-based conservation and management decisions.

The Johannesburg Plan of Implementation [*United Nations*, 2002] describes the need for increased collaboration and transfer of knowledge in marine science, technology, conservation, and management in Africa, where many coastal nations rely heavily on marine resources. Development of decision support tools for marine resource management is therefore a top priority of the Intergovernmental Oceanographic Commission (IOC) of the United Nations Educational, Scientific, and Cultural Organization (UNESCO) and forms part of UNESCO's Priority Africa initiative [*IOC*, 2009] (UNESCO-IOC, personal communication, 2009). Decision support tools can be complex as they must model various interdependent processes relevant to marine resource management, such as economic, biological, and physical processes. Numerical models of the relevant dynamics of the coastal ocean can be one integral part of these decision support tools. This paper presents such a numerical model of the seasonal and tidal dynamics of the Zanzibar Channel, referred to as the Zanzibar Channel Model (ZCM). It serves as an example of numerical models that could be used to develop decision support tools for marine resource management in Tanzania, where one-third of the national gross domestic product is produced in the country's coastal region. The results presented in this

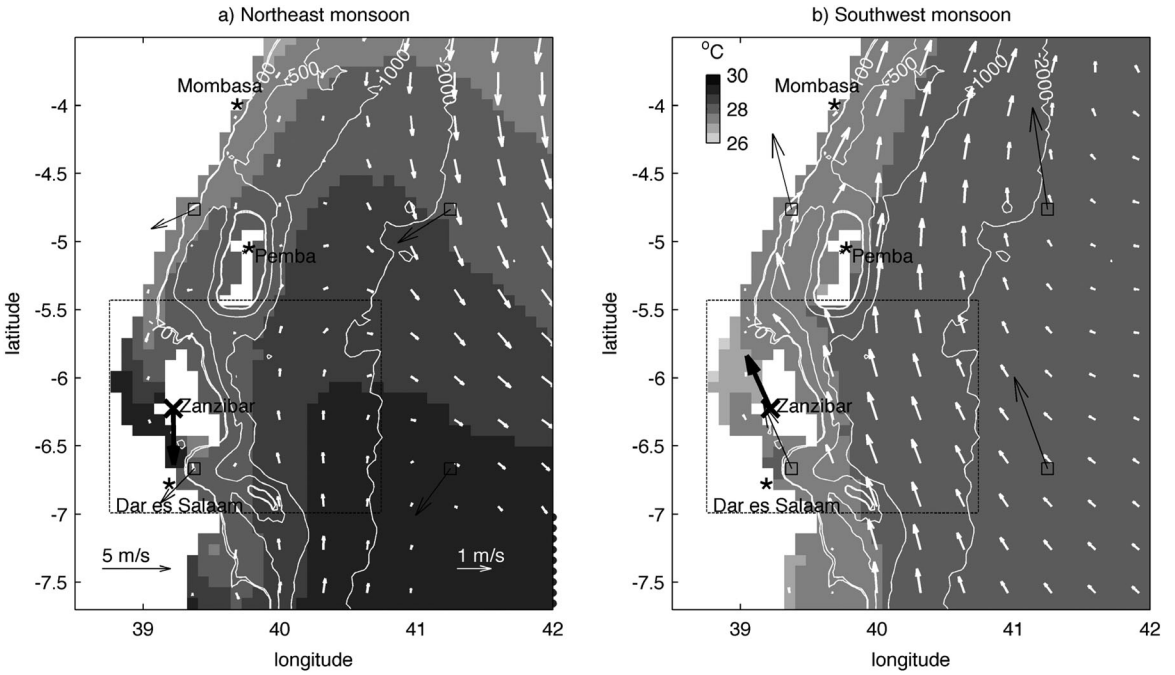

Figure 1. Large-scale dynamics in the wider area of the Zanzibar Channel. The white contour lines show the 70, 100, 500, 1000, and 2000 m isobaths of the bathymetry. (a) The large-scale dynamics in February, during the northeast monsoon season, and (b) in June, during the southwest monsoon season, is shown. The filled contours and white arrows show HYCOM monthly means of the SST and surface velocity field, respectively. The black arrows show the wind. At the squares they show the NCEP reanalysis monthly mean wind and at the cross they show the monthly mean wind measured at the Chukwani meteorological station. The dotted box indicates the ZCM's domain.

paper were obtained through a collaboration between United States and Tanzanian scientists, students, and technicians. In particular, the students from the United States were from 12 different universities and conducted modeling studies and field work at the Institute of Marine Sciences on Zanzibar Island in the austral winters of 2009, 2010, and 2011.

The Zanzibar Channel (Figure 1) is located in the tropical western Indian Ocean at about 6°S and 39°E, and lies on the continental shelf of the coastal ocean of Tanzania between the mainland and Zanzibar Island. The channel is about 100 km long, 40 km wide, and 40 m deep [*Shaghude and Wannäs*, 1998]. At the two channel openings, the depth drops steeply to greater than 1000 m (Figure 2). The dominant large-scale

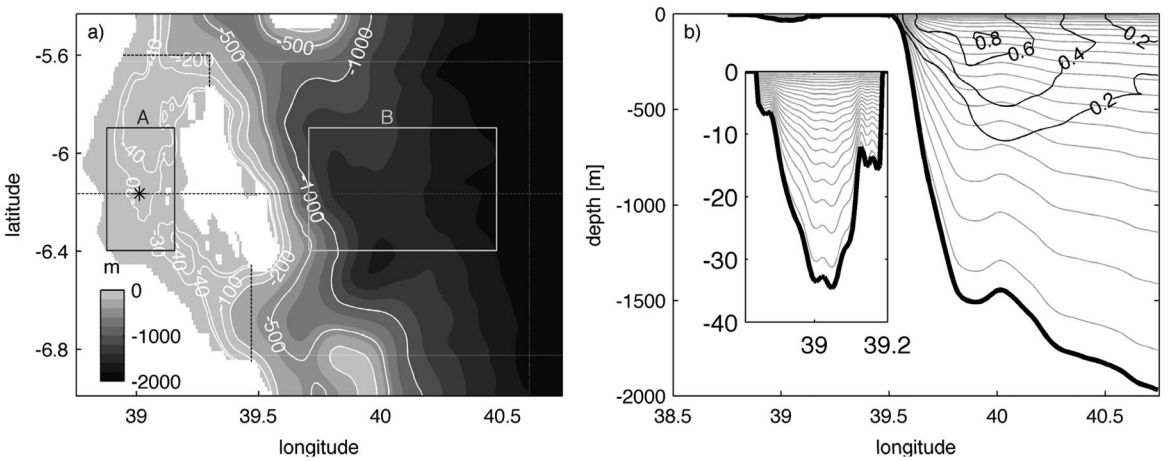

Figure 2. ZCM bathymetry and vertical discretization. (a) The ZCM bathymetry (filled contours) and its 30, 40, 100, 200, 500, and 1000 m isobaths (white contour lines) are shown. The width of the nudging layer is indicated by the white dotted lines. The spatial means of temperature, mentioned in section 3.3, are calculated inside boxes A and B. The average kinetic energies, mentioned in section 4.3, are calculated inside the area enclosed by the black dotted lines at both Zanzibar Channel openings. The black-dotted line indicates the latitude of the vertical section shown in Figure 2b, depicting the 20 terrain-following levels (thin gray lines). (b) The core of the northward-flowing EACC is shown by depicting the 0.2, 0.4, 0.6, and 0.8 m/s contours of its annual mean meridional velocity component (thick gray contour lines). The inset in Figure 2b shows a magnification of the vertical section through the Zanzibar Channel.

dynamical features that impact the dynamics of the Zanzibar Channel are the East African Coastal Current (EACC) and the local monsoon wind, both shown in Figure 1 [e.g., *Shetye and Gouveia*, 1998; *Schott et al*., 2009]. The EACC flows northward throughout the year predominantly along the eastern side of Zanzibar Island with only a very small portion flowing through the Zanzibar Channel, which is evident by the channel's shallow depth compared to that of the ocean east of Zanzibar Island, as shown in Figure 2b [e.g., *Newell*, 1957; *Swallow et al*., 1991]. The local monsoon wind in the Zanzibar Channel varies seasonally: the wind tends to be northerly during the northeast monsoon season from December to February, and southeasterly during the southwest monsoon season from April to November [e.g., *Hellerman and Rosenstein*, 1983; *Ngusaru and Mohammed*, 2002; *Mahongo et al*., 2011].

Several aspects of the dynamics of the Zanzibar Channel have been studied previously. For example, some features of its tidal dynamics have been identified [e.g., *Shaghude et al*., 2002; *Mahongo and Francis*, 2010], and the local dynamics near coral reefs have been studied at several locations [e.g., *Muzuka et al*., 2010]. This paper complements these previous studies by presenting the seasonal and tidal dynamics of the ZCM and showing that the dynamics is consistent with observations. Moreover, it demonstrates that the ZCM can be used to study the dispersion of passive tracers, a line of inquiry yet to be pursued despite the local societal and environmental importance of predicting the dispersion of sewage pollution or coral larvae.

In this paper, the development of the ZCM using the Regional Ocean Modeling System (ROMS) is described in section 2. The observations, accompanied by their comparison with the ZCM, are presented in section 3. The dominant features of the modeled seasonal and tidal dynamics are described in section 4. The ZCM simulation of passive tracer dispersion is presented in section 5 as one example of potential model applications. A concluding discussion is provided in section 6.

2. Model

The ZCM is based on ROMS, a numerical three-dimensional ocean circulation model developed specifically for regional ocean applications [*Haidvogel et al*., 2000, 2008, www.myroms.org]. It solves the Reynolds-averaged Navier-Stokes equations using the hydrostatic and Boussinesq approximations, employs split-explicit separation of fast barotropic and slow baroclinic modes, and is formulated in vertically stretched, terrain-following, *s*-coordinates. ROMS includes high-order advection and time-stepping schemes, weighted temporal averaging of the barotropic mode to reduce aliasing into the slow baroclinic modes, and conservative parabolic splines for vertical discretization. A barotropic pressure-gradient formulation reduces the pressure-gradient truncation error that previously has limited the accuracy of the terrain-following coordinate models [*Shchepetkin and McWilliams*, 2005]. Momentum, scalar advection, and diffusive processes are represented using transport equations, while the vertical velocity is computed diagnostically, using volume conservation. *Shchepetkin and McWilliams* [2003, 2005, 2009] describe in detail the algorithms that comprise the ROMS computational kernel.

The ZCM domain (box in Figure 1) is large enough to capture adequately the large-scale processes affecting the dynamics in the channel, and to allow the use of the output of global Ocean General Circulation Models (OGCMs) and global ocean tidal models for the forcing at the lateral boundaries. The domain extends from Tanzania's mainland coast out to the deep ocean at 40.8°E and from 7°S to 5.4°S. The model bathymetry is a smoothed version of the bathymetry obtained from the General Bathymetric Chart of the Oceans (GEBCO) One Minute Grid, version November 2008 (www.gebco.net). Smoothing is necessary to minimize the pressure-gradient errors associated with *s*-coordinate models. The spatial resolution is sufficiently fine to model the seasonal dynamics and the tides. It varies from approximately 2 km at the ZCM's lateral boundaries to approximately 1 km inside the channel. In the vertical, the ZCM has 20 terrain-following levels with resolution increasing gradually toward the surface, where the average vertical resolution is 0.25 m. Figure 2b shows the vertical resolution for the cross section along the central black dotted line in Figure 2a. At the cross section's deepest location in the channel, its vertical resolution is coarsest, increasing from 5.4 m near the bottom to 0.35 m near the surface.

The bottom friction formulation used in the ZCM has a quadratic drag coefficient in the bottom stress boundary condition that is proportional to $1/\ln^2(z/Z_{ob})$, as proposed by *Warner et al*. [2005, 2008], where z is the elevation above the bottom of the lowest vertical grid point and Z_{ob} is a constant bottom roughness length. The Zanzibar Channel seafloor consists of fine to coarse sand with ripples, with coral reefs in some

shallow regions [*Shaghude and Wannäs*, 1998, 2000]. A roughness length of $Z_{ob}=2$ cm was chosen based on an approximate average roughness for the ripples and reefs, which is larger than the measured value of about 0.6 cm for sandy ripples alone [*Salon et al*., 2011]. For the turbulence closure scheme, the Generic Length Scale (GLS) turbulence closure model was used with its parameters set such that it represents the $k-\epsilon$ parameterization [*Jones and Launder*, 1972; *Launder and Sharma*, 1974; *Rodi*, 1984; *Warner et al*., 2005]. For the incoming solar radiation, ROMS uses the double-exponential profile for shortwave radiation absorption as fitted by *Paulson and Simpson* [1977] to the data of *Jerlov* [1968]. The water type I, as defined by *Jerlov* [1968], was selected because it represents clear waters such as those of the Zanzibar Channel.

On the lateral boundaries, the ZCM was forced with the seasonal cycles of monthly means of temperature and salinity from 2000 to 2007 provided by an OGCM, the data-assimilative Hybrid Coordinate Ocean Model (HYCOM) [*Bleck*, 2002]. These monthly means were adjusted using the method proposed by *Killworth* [1996], such that when the forcing is linearly interpolated by ROMS, the monthly means resulting from the interpolation are identical to the original monthly means. A correction to the HYCOM vertical temperature profile above 100 m depth, which is the approximate depth of the climatological thermocline, was made by shifting the profile such that the seasonal cycle of the surface value of the shifted profile was always identical to the seasonal cycle of the sea surface temperature (SST) of the 7-day composite Coral Reef Temperature Anomaly Database (CoRTAD) SST analysis, version 4 [*Selig et al*., 2010], which provides SST at an approximately 4 km resolution from 1982 to 2010. At 100 m depth, this shifted profile was smoothly ramped to the HYCOM profile below 100 m depth. This temperature correction was necessary to achieve more accurate forcing, because while the HYCOM and CoRTAD SSTs are consistent for most of the year, the HYCOM SST has a warm bias of about 1°C relative to the CORTAD SST, but only during the austral winter months. Another OGCM, the Ocean General Circulation Model For the Earth Simulator (OFES) [*Masumoto et al*., 2004; *Sasaki et al*., 2008], was considered but was not used because the OFES SST has a persistent cold bias of about 1°C relative to the CoRTAD SST throughout the full seasonal cycle.

The temperature and salinity of the ZCM are nudged to the temperature and salinity of the lateral boundary forcing, following the approach used by *Bryan and Holland* [1989], and in addition adopting the adaptive open boundary conditions proposed by *Marchesiello et al*. [2001]. The adaptive open boundary conditions allow the nudging at the lateral boundaries to be strong with the nudging time scale chosen to be 5 days when fluxes are oriented into the ZCM domain, and weak with the nudging time scale chosen to be 50 days when fluxes are oriented out of the ZCM domain. Adjacent to the lateral boundaries inside the ZCM domain, a nudging layer with a thickness of ten grid points, which represents 15 km on the eastern boundary and 22 km on the southern and northern boundaries, as shown by the white dotted lines in Figure 2a, was implemented. In this nudging layer, the nudging time scale is chosen to decrease linearly from 5 days at the lateral boundaries to zero on the other side of the nudging layer. The strong nudging does not lead to unwanted accumulation of energy in the ZCM, despite results cautioning that this may occur [*Marchesiello et al*., 2001]. The option to nudge only temperature and salinity was chosen so that the ZCM internal dynamics can determine all other variables, resulting in a dynamical consistency among all variables. This was necessary because the correction to the temperature profile of the lateral boundary forcing destroyed the consistency among all variables of the lateral boundary forcing, as it exists, e.g., in thermal wind balance.

Chapman [1985] and *Flather* [1976] boundary conditions were imposed at the lateral boundaries for the sea surface height and the barotropic velocity respectively, both representing the barotropic component of the dynamics. These formulations allow gravity waves to radiate out of the ZCM domain, and allow the tidal dynamics, which is not described by the lateral boundary forcing provided by HYCOM, to be forced at the lateral boundaries. The six most dominant tidal constituents observed in the channel by *Mahongo and Francis* [2010] were forced using the global Oregon State University (OSU) tidal data inversion [*Egbert et al*., 1994].

At the surface, the ZCM was forced with seasonal cycles of air-sea momentum, heat, and freshwater surface fluxes, determined using the bulk formulae parameterizations of *Fairall et al*. [2003]. The atmospheric fields required by these parameterizations are provided by a spatial linear interpolation combining seasonal cycles based on two different data sets. One are measurements of monthly means of rainfall, air temperature, air pressure, and wind from the Chukwani meteorological station near the Zanzibar airport (cross on Zanzibar Island in Figure 1) [*Mahongo and Francis*, 2010] from 1985 to 2004. The other are monthly means of the NCEP reanalysis [*Saha et al*., 2010] at the four grid points nearest to Zanzibar Island (squares in Figure 1) from 1949 to 2009. The atmospheric fields are spatially fairly uniform mainly because of the flat

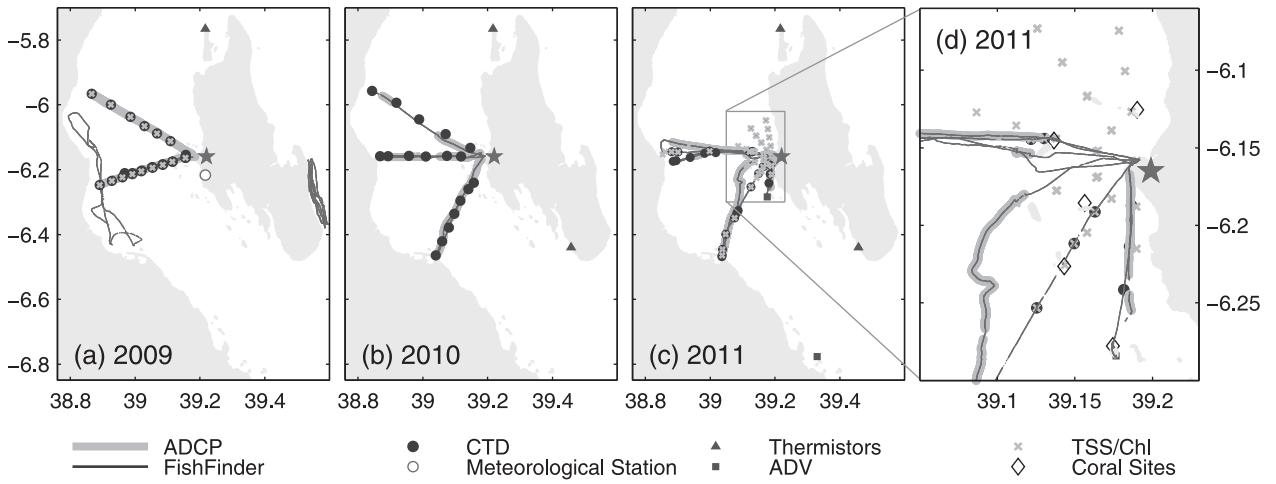

Figure 3. Observation locations and instruments used in 2009, 2010, and 2011. The locations of all observations that were made in 2009 are shown in Figure 3a, in 2010 in Figure 3b, and in 2011 in Figures 3c and 3d. The instruments used are listed below the plots. Table 1 lists the variables that were measured by the instruments as well as the depths and durations of these measurements. The thick gray lines indicate dhow tracks of cruises only from Stone Town (star), while the thin black lines indicate dhow tracks of cruises that both left from and returned to Stone Town. The Meteorological Station marked by a circle is the Chukwani meteorological station near the Zanzibar airport. The diamonds indicate the five sites where photographs of coral reefs near small islands were taken. These islands are, listed from north to south: Chapwani and Bat, Bawe, Pange, Nyange, and Chumbe.

topography of Zanzibar Island and the mainland and thus well represented by the NCEP reanalysis despite its coarse resolution. Furthermore, the Chukwani meteorological station provides direct observations at a location closer to the Zanzibar Channel than the NCEP reanalysis at any of its grid points, thus including these observations is expected to improve the seasonal cycles of monthly means of the various variables. The monthly means were adjusted in exactly the same fashion as the monthly means at the lateral boundaries, using the method proposed by *Killworth* [1996].

The ZCM was initialized with the January mean of the seasonal cycle of HYCOM with the temperature correction applied and integrated for 4 years with a barotropic time step of 1 s and a baroclinic time step of 50 s. After spinning up for 1 year, the ZCM reached a limit cycle. The fourth year of the integration is presented in this paper.

3. Observations and Comparison With the Model

The observations, summarized in Figure 3 and Table 1, were collected from 2009 to 2011. A dhow, which is a traditional wooden sailboat ubiquitous in the western Indian Ocean region, was equipped with various oceanographic instruments and used as the platform for most of the observations. Cruises on the dhow were undertaken during daylight hours and were organized as transects across the channel. On cruises from Stone Town on Zanzibar Island toward the Tanzanian mainland (thick lines in Figure 3), the dhow traveled at constant speed along the transects while vertical profiles of velocity for the full water column were measured continuously, using a 600 kHz RDI Workhorse Sentinel ADCP attached to the dhow with a "New Kentucky" mount (D. S. Mueller, personal communication, 2009, and http://hydroacoustics.usgs.gov/movingboat/pdfs/KYMount.pdf). At specific locations on the return cruises back to Stone Town (dots in Figure 3), vertical profiles of temperature and salinity for the full water column, using a SBE 19 SEACAT Profiler CTD, and chlorophyll-a concentrations were measured. On all cruises, the water depth and surface

Table 1. Observation Durations and Instruments Used in 2009, 2010, and 2011

Measurement	Instrument	Location in Figure 3 and Depth	Duration
Velocity and depth	ADCP	Along ▬ from surface to bottom	7 days
Temperature, salinity and depth	CTD	At ● from surface to bottom	7 days
Temperature and depth	Fishfinder	Along ——— at surface	19 days
Temperature	Thermistor	At ▲ at 5 and 15 m	19 months
Velocity and pressure	ADV	At ■ at bottom	31 days
Coral coverage	Camera	At ◇ at bottom	3 days
Total suspended solids	Scale	At × at surface	5 days
Chlorophyll-a	Spectrophotometer	At × at surface	6 days

temperature were measured continuously by a Garmin GPSMAP 420S Fishfinder equipped with a dual beam/frequency transducer (thick and thin lines in Figure 3). In addition to the transect measurements, temperature was measured at two locations (triangles in Figure 3) during 2009–2011 by deployed HOBO Pendant Temperature/Alarm Data Logger 8 K thermistors, resulting in 1.5 years of temperature records at each location. In 2011, additional measurements were taken. Velocity and pressure were measured continuously at two locations at the bottom of the channel (squares in Figure 3c) for 14 and 17 days at each location by a SonTek Triton ADV. The status of coral reefs was recorded by taking photographs at five sites near small islands near Stone Town (diamonds in Figure 3d). Total suspended solids (TSS) and chlorophyll-a concentrations were measured during daylight at locations on arcs centered at Stone Town (crosses in Figures 3c and 3d) for 5 and 2 days, respectively.

3.1. Bathymetry

The ZCM bathymetry was compared with bathymetric observations to ensure the accuracy of the ZCM bathymetry, which strongly constrains the simulated flows and barotropic tidal phase speed. Along the cruise tracks in the Zanzibar Channel, the water depth was measured by the Fishfinder, and usually was simultaneously measured by the ADCP. The Fishfinder and ADCP water depth measurements are in close agreement; the root-mean-square (RMS) difference between the Fishfinder and ADCP measurements is 1.6 m. Because of this excellent agreement, only the water depth measured by the Fishfinder was used. The observed bathymetry was computed from the water depth measurements by removing the tidal elevation using harmonic analysis of the ZCM. In order to compare the observed bathymetry with the ZCM bathymetry, the bathymetry observed in a particular ZCM grid cell was averaged over the area of the grid cell and compared with the ZCM bathymetry of this grid cell. The comparison is shown in Figure 4. The correlation is 0.9, the bias 3.6 m, and the RMS difference 6.1 m. The largest differences are in areas with strong bathymetric gradients.

3.2. Velocity

The vertical profiles of velocity measured by the ADCP along transects and the corresponding profiles of the ZCM allow for two comparisons. One is a comparison of the vertically averaged horizontal velocity fields and the other of the horizontally averaged vertical profiles of the meridional velocity component.

For the comparison of the vertically averaged horizontal velocity fields, the vertical profiles of velocity were vertically averaged and horizontally averaged over a distance equivalent to the ZCM's horizontal resolution. The result, presented in Figure 5, shows the measured and modeled horizontal velocity fields in the top and bottom rows, respectively. The comparison of the measured and modeled zonal velocity components gives a correlation coefficient of 0.9, a bias of 1 cm/s, and an RMS difference of 4 cm/s and the comparison of the measured and modeled meridional velocity components gives a correlation coefficient of 0.79, a bias of −3 cm/s, and an RMS difference of 8 cm/s. The changes in flow directionality observed in most of the transects is due to the evolution of the tidal phase during the periods of several hours in which the velocity measurements were made. These flow directionality changes are prominent because the tidal flow is the largest component of the total flow.

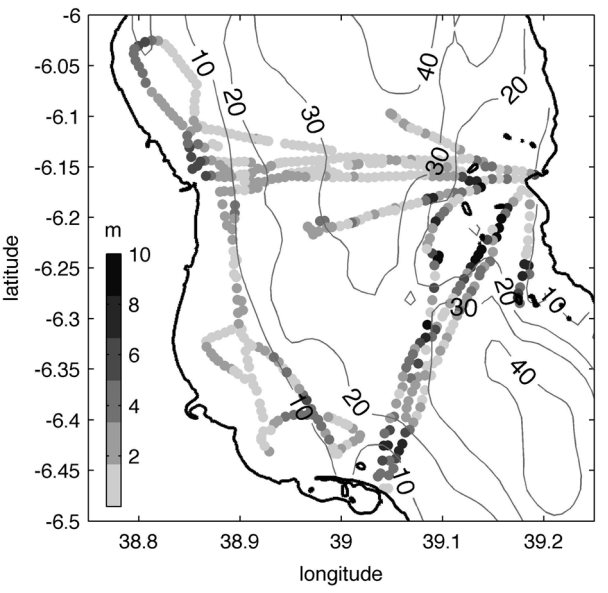

Figure 4. Comparison of the observed and ZCM bathymetries. The ZCM bathymetry is shown by contour lines. The difference between the observed and ZCM bathymetry is shown by dots at the observation locations. The RMS difference of 6.1 m.

For the comparison of the horizontally averaged vertical profiles of the meridional velocity component, the tidal component

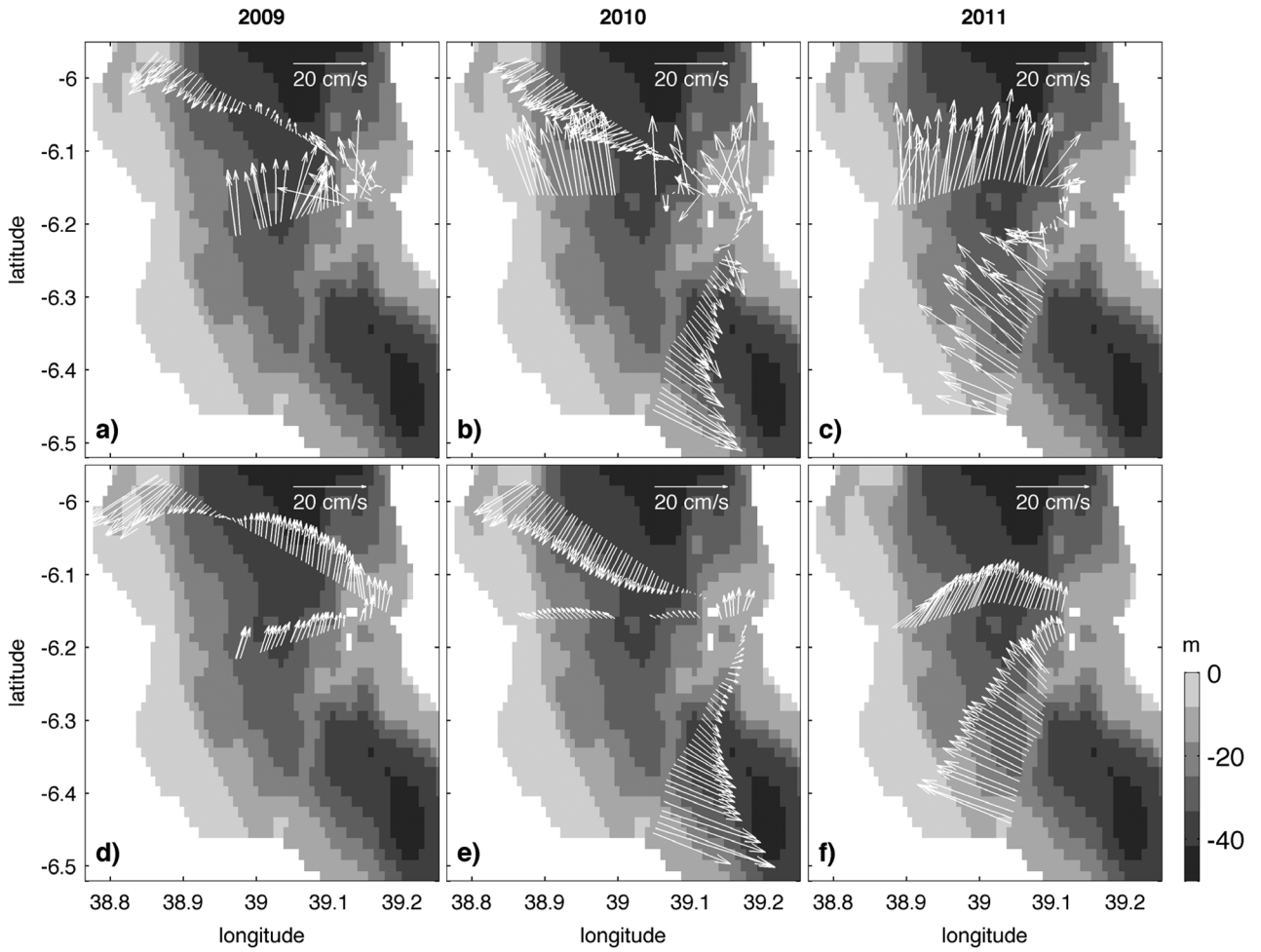

Figure 5. Comparison of the observed and ZCM depth-averaged horizontal velocity fields. The vertical profiles of velocity measured along transects (thick gray lines in Figure 3) and the corresponding ZCM profiles were averaged vertically and horizontally over a distance equivalent to the ZCM horizontal resolution. The resulting velocity fields obtained from the measurements made in 2009 are shown in Figure 5a, in 2010 in Figure 5b, and in 2011 in Figure 5c. The corresponding ZCM velocity fields are shown in Figures 5d–5f, respectively. Since it took about 5 h to measure the vertical profiles of velocity along each transect, the measurements captured different phases of the tide, which causes the apparent flow direction changes along the transects.

had to be removed. Because of the limited number of measured profiles, the tidal component cannot be completely removed by averaging horizontally. Instead, a different approach was used. Measured profiles that extend beyond 20 m depth were selected. The mean below 15 m depth of each profile was calculated and subtracted from that profile. Since it was assumed that below 15 m the flow consists only of the remotely forced and tidal flows, this subtraction removed the tidal component from each profile, as desired, but also the component of the remotely forced flow having a constant vertical profile below 15 m. To compensate for the loss of this remotely forced flow component, a flow component with a constant vertical profile and a magnitude of 9 cm/s was added, where the magnitude was estimated by using ZCM profiles that extend beyond 20 m depth along the dotted black line across the channel in Figure 2a during the period from June to August. The horizontal average of the resulting profiles is depicted by circles in Figure 6. The standard deviation, which is largely depth invariant, is on the order of 2.3 cm/s. The modeled horizontally averaged vertical profiles of the meridional velocity component, resulting from all the profiles that extend beyond 20 m depth along the dotted black line across the channel in Figure 2a, were calculated straightforwardly by averaging them horizontally for four different 3-month periods of the year, thus reducing the tidal component substantially. The four profiles are shown by lines in Figure 6. The standard deviation of all four profiles combined, which is also largely depth invariant, is on the order of 1.7 cm/s. Despite the limited number of observations, the observed and modeled profiles agree well, which is most likely attributed to the steady southeasterly wind and the steady remotely forced flow during the austral winter months.

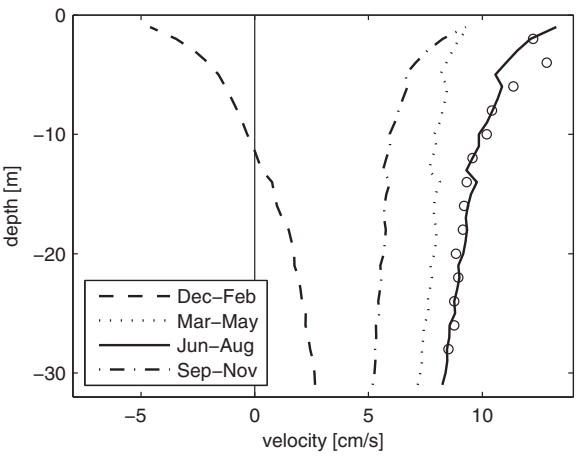

Figure 6. Vertical profiles of the meridional velocity component. The vertical profiles of velocity measured along transects (thick gray lines in Figure 3) were averaged horizontally in a particular manner described in section 3.2 and the resulting average vertical profile of the meridional velocity component is shown by the circles. The ZCM average vertical profiles of the meridional velocity component were obtained from vertical profiles of velocity on the black-dotted line in the Zanzibar Channel in Figure 2a for four 3-month periods of the year and are shown by four different lines explained in the legend.

Velocity was also measured by an ADV deployed at the bottom near Chumbe Island (northern square in Figure 3c) for 15 days. Figure 7 compares the measured and modeled zonal (top plot) and meridional (bottom plot) velocity components. The means of the measured and modeled zonal velocity components are −2.4 cm/s and −2.2 cm/s, respectively. The correlation coefficient for the measured and modeled zonal velocity components is 0.5, and the RMS difference 5 cm/s. The means of the measured and modeled meridional velocity components are 3.1 cm/s and 2.4 cm/s, respectively. The correlation coefficient for the measured and modeled meridional velocity components is 0.8, and the RMS difference is 6 cm/s. While there is good agreement in the phase and amplitude of the meridional velocity components, the amplitude of the zonal velocity component is overestimated by the ZCM, which is a relatively minor deficiency since it is smaller than the meridional velocity component. The overestimation could be due to a difference in actual and modeled bathymetries at the location the ADV was deployed, which was the western slope of Chumbe Island. The slope's isobaths are nearly meridional and since the slope is fully exposed to the open channel, a good agreement between the measured and modeled meridional velocity components can be expected. However, in the zonal direction toward the east, Chumbe Island represents an actual barrier, while in the ZCM Chumbe Island is not resolved and a shallow ocean is in its place, making it plausible that the ZCM would overestimate the zonal velocity component.

3.3. Temperature and Salinity

A comparison of the seasonal cycles of SST given by CoRTAD and the ZCM is shown in Figure 8 for spatial averages inside (left plot) and outside (right plot) the channel, where inside and outside the channel is

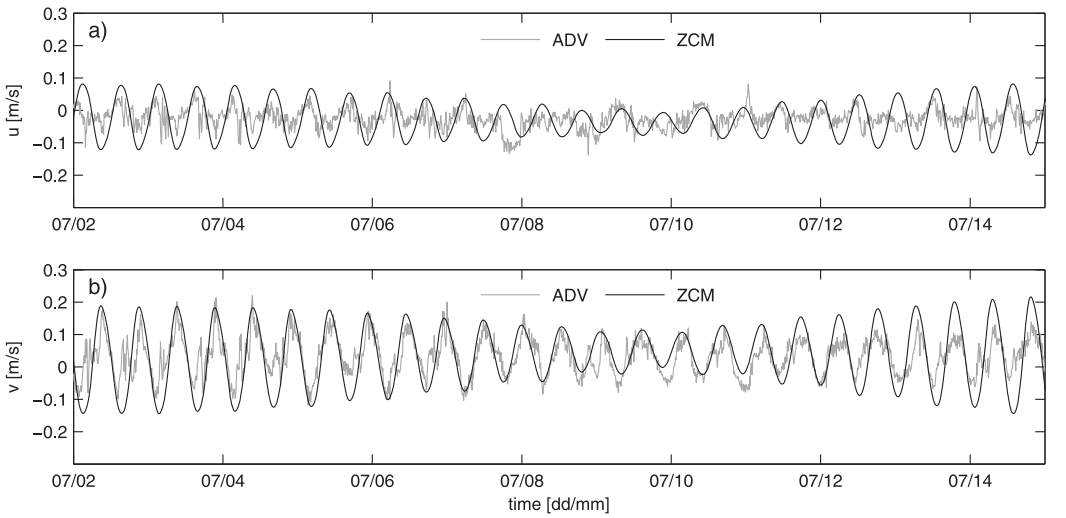

Figure 7. Comparison of the observed and ZCM velocity near Chumbe Island. The velocity measured near Chumbe Island (northern square in Figure 3c) is shown by the gray lines and the corresponding ZCM velocity by the black lines, where their respective zonal velocity components are shown in Figure 7a and meridional velocity components in Figure 7b. The tidal ellipse derived from the measured velocity is shown in Figure 13 and labeled "ADV."

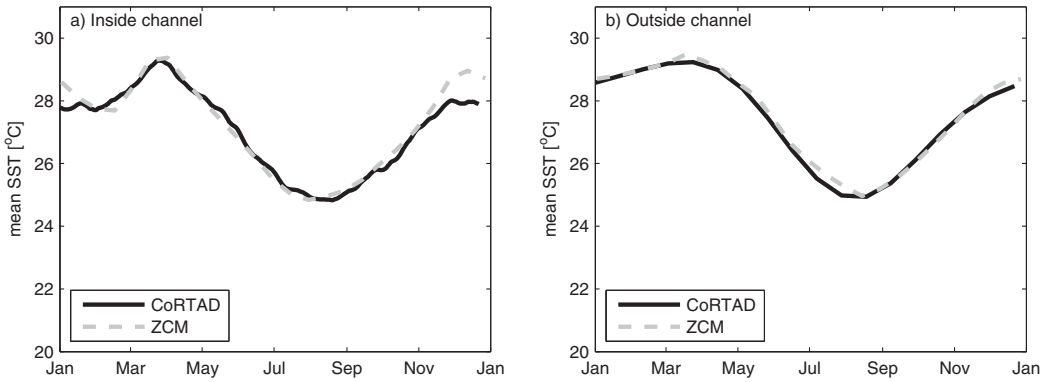

Figure 8. Comparison of the observed and the ZCM seasonal cycles of SST. (a) The spatial means of the SSTs of CoRTAD (black line) and the ZCM (dashed line) inside the Zanzibar Channel, as defined by box A in Figure 2, and (b) outside the channel, as defined by box B in Figure 2, are shown. A temporal cooling during the period from December and February is evident in the SST of both CoRTAD and the ZCM. The difference in the respective evolutions of this temporal cooling could be due to interannual variability because the seasonal cycle of the SST of CoRTAD is obtained from different range of years than the seasonal cycles used to force the ZCM.

defined by boxes A and B in Figure 2a, respectively. The excellent agreement between the observed and modeled temperature suggests that the temperature correction made in the forcing at the lateral boundaries, as described in section 2, was appropriate. The only noticeable disagreement occurs inside the channel between December and January. This time period coincides with a temporal cooling period seen by both the CoRTAD and ZCM SSTs, where the onset of the cooling period occurs earlier in the observations than in the model. *Muhando* [2002] observed this temporal cooling near Bawe and Chumbe Islands, shown in Figure 3, from 1997 to 2002, and noted that the temperature measurements exhibited a larger interannual variability during the cooling period than during the remainder of the year. This enhanced interannual variability is likely the reason for the disagreement between the CoRTAD and ZCM SSTs during the cooling period because the seasonal cycles of the CoRTAD SST was determined from a different range of years than the ranges of years that were used to determine the various seasonal cycles used in forcing the ZCM.

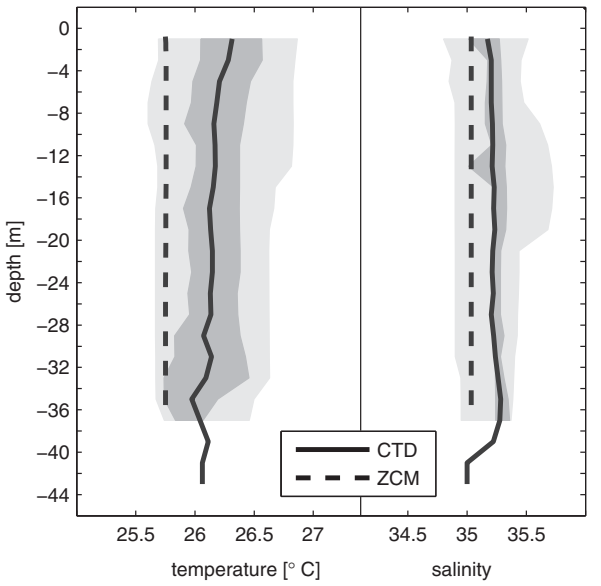

Figure 9. Comparison of the observed and ZCM vertical profiles of temperature and salinity. All observations were made in July and August in 2009, 2010, and 2011. The statistics of all 66 vertical profiles of both temperature and salinity measured at the locations indicated by the large black dots in Figure 3 are presented by their means (solid lines), 25–75 percentile ranges (dark gray area), and entire ranges (light gray area). The means of the corresponding ZCM profiles are shown by dashed lines, but the ranges are too small to be shown. The standard deviation of the temperature profiles is only 0.1°C and of the salinity profiles only 0.06. The profiles indicate a well-mixed channel.

The statistics of all 66 vertical profiles of temperature and salinity measured by the CTD and the corresponding profiles of the ZCM are compared in Figure 9. The means of the measured profiles are shown by the solid lines and the 25 and 75 percentile ranges are shown by the dark and light gray areas, respectively, but only at depths at which more than 25 profiles were measured. The means of the modeled profiles are shown by the dashed lines, but the 25 and 75 percentile ranges are not shown because they are too small. The standard deviation of the temperature profiles is only 0.1°C and of the salinity profiles only 0.06. The mean of the temperature increases toward the surface by about 0.1°C, which is most likely a biased increase because measurements were only taken during the day. Figure 9 primarily indicates that the channel is well

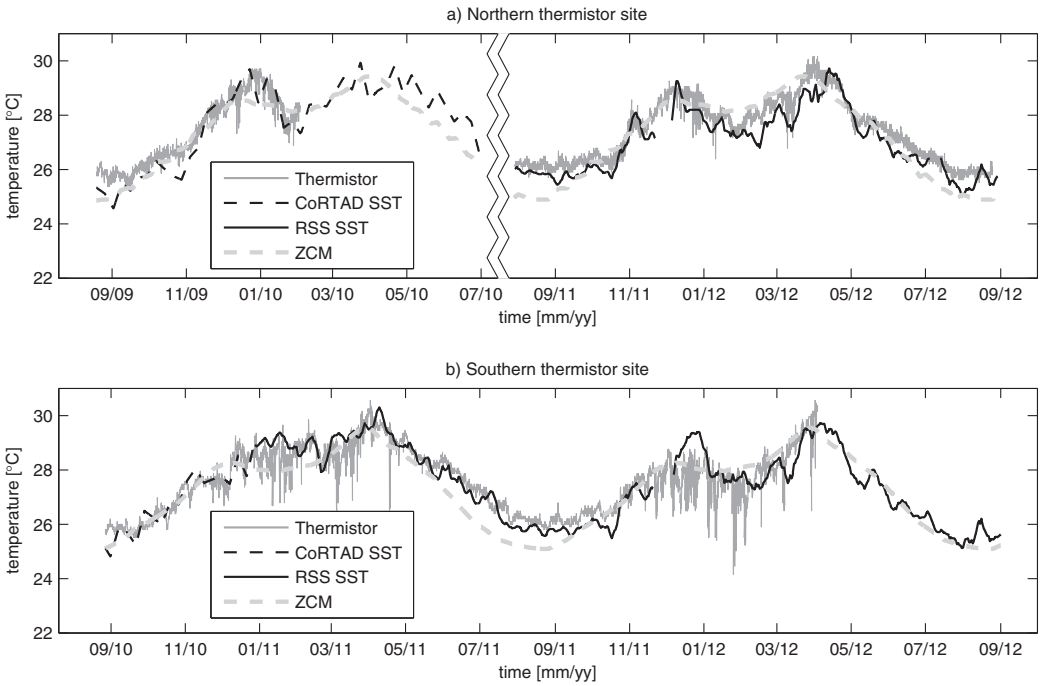

Figure 10. Comparison of the observed and ZCM temperature. The temperatures at the northern and southern sites, where thermistors were deployed (triangles in Figure 3), are shown in Figures 10a and 10b, respectively. The temperature measured by the thermistors is shown by dark gray solid lines, the CoRTAD and RSS SSTs by black dashed and solid lines, respectively, and the 5-day mean ZCM temperature by light gray dashed lines.

mixed during the austral winter. This becomes even clearer by inspecting the individual measured vertical profiles (not shown), which reveals that they vary little with depth, only by about ± 0.5°C and ± 0.2, respectively.

Temperature was also measured nearly continuously from 2009 to 2012 by thermistors at two locations in the north and south of the eastern side of the Zanzibar Channel (triangles in Figure 3). Three thermistors were deployed in close proximity to each other inside coral reefs at depths of 5 m or 15 m at each of the two locations for about 6 months at a time. If more than one was recovered, the mean of the simultaneous measurements was used for the analysis, reducing the instrument error. Roughly 1.5 seasonal cycles were recorded at each location, though not for the same time periods. They are presented by the gray solid lines in Figure 10. The corresponding 5-day mean temperature of the ZCM is shown by the gray dashed line. The comparison of the 5-day mean of the measured temperature, which represents the seasonal cycle since higher frequency variations are removed by the 5-day mean, with the modeled temperature, gives a correlation coefficient of 0.93, a bias of -0.25°C, and an RMS difference of 0.5°C.

Another comparison of the temperature measured by the thermistors can be made with the temperature measured by satellites, given by CoRTAD SST until 2010 and the 1-day composite of the multisatellite blended SST analysis from Remote Sensing Systems (RSS) beyond 2010 (data available at www.misst.org). Both CoRTAD and RSS SSTs are shown in Figure 10 by the black dashed and solid lines, respectively. This comparison gives a correlation coefficient of 0.92, a bias of -0.13°C, and an RMS difference of 0.6°C.

The thermistors and satellite temperature observations show the temporal cooling for specific years. At the northern location, for example, the onset of the temporal cooling in 2010 is in January, while in 2012 it is a month earlier in December 2011. The different times of the onset lend further support to the previous findings mentioned above that the temporal cooling varies interannually.

3.4. Pressure

Observed pressure, equivalent to observed sea level, allows the tidal dynamics at the sample location to be determined and compared with the corresponding tidal dynamics of the ZCM. For this study, observed pressure was available at three different locations in the Zanzibar Channel.

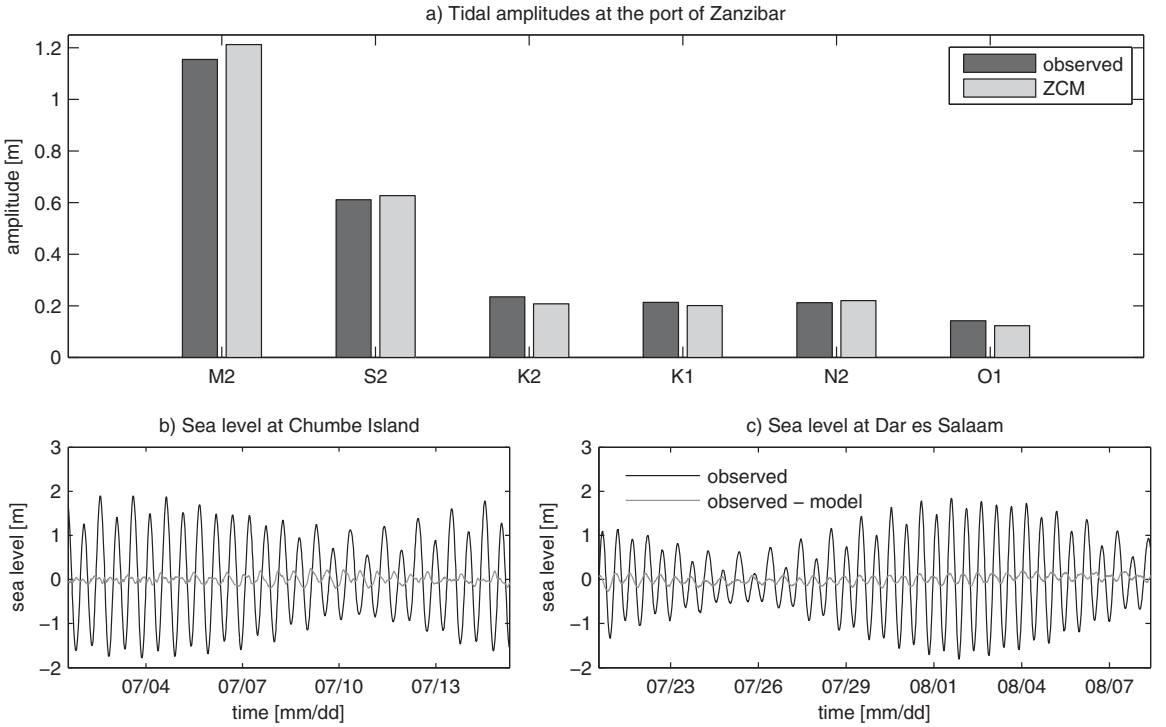

Figure 11. Comparison of the observed and ZCM tidal amplitudes and sea levels. (a) The tidal amplitudes of the six most dominant tidal constituents at the port of Zanzibar (star in Figure 3) determined from sea level measurements (black bars) and from the corresponding ZCM sea levels (gray bars) are shown. (b and c) The measured sea level (black lines) and the difference between the measured and corresponding ZCM sea levels (gray lines) near Chumbe Island (northern square in Figure 3c) and Dar es Salaam (southern square in Figure 3c) are shown.

At the port of Zanzibar (star in Figure 3), 25 years of hourly sea level measurements were available and provided by the University of Hawaii Sea Level Center [*IOC*, 2012]. Using harmonic analysis, the amplitudes of those six tidal constituents with which the ZCM was forced at its lateral boundaries, as described in section 2, were determined. They are shown by black bars in Figure 11a. For comparison, the corresponding amplitudes of the ZCM, estimated using harmonic analysis of eight months of hourly sea surface height at the closest model grid point, are shown by the gray bars. There are only some small discrepancies between the observed and modeled amplitudes, with the ZCM slightly overestimating the main two semidiurnal tidal constituents M2 and S2.

At the other two locations near Chumbe Island in the east and Dar es Salaam in the west of the channel (squares in Figure 3c), pressure was measured in 2011 by the ADV for 14 and 17 days, respectively. The corresponding sea level is shown by the black lines in Figures 11b and 11c, respectively. Because the corresponding sea level of the ZCM would be visually indistinguishable from the measured sea level, the difference between the two is shown instead by the gray lines in Figures 11b and 11c. The difference represents just 5% of the total observed variability.

3.5. Status of Coral Reefs, Total Suspended Solids, and Chlorophyll-a

The purely physical observations presented above are complemented by observations related to the biology of the Zanzibar Channel presented in this section. They, too, are compared with the ZCM, but this is deferred to section 5 as the comparison requires the discussion of the dynamics of the Zanzibar Channel, which is presented in section 4. The observations presented in the following were made in July and August 2011, unless indicated otherwise.

To assess the status of the coral reefs, the reef assemblages at five sites located near small islands were observed. The sites' locations are shown by diamonds in Figure 3d and the nearby islands, listed from north to south, are Chapwani and Bat, Bawe, Pange, Nyange, and Chumbe. At each of two stations chosen at each site seven random 1 m $\times$ 1 m quadrants were photographed with a Canon PowerShot SX200 IS with a 28 mm wide-angle lens. The camera was attached to a 1 m $\times$ 1 m PVC-frame [*van Woesik et al.*, 2009]. The photographs were analyzed using CPCe software and 10 random points per image [*Kohler and Gill*, 2006] to

determine in particular the percentage of the reef area that was covered by corals, or short, the coral cover, of the dominant coral genera *Acropora* and *Porites*.

Although the health of a reef is difficult to quantify, past studies have shown that land use change, thermal stress, and pollution all stress *Acropora* corals more so than *Porites* corals [*van Woesik et al*., 1999; *Golbuu et al*., 2011]. *Acropora* are highly reliant on the photosynthetically derived glycerol supply from their endosymbionts, and those symbionts are sensitive to changes in the environment. In contrast, *Porites* corals are more tolerant to disturbances. Therefore, coral cover and the ratio of coral cover of *Acropora* and *Porites* are indictors of reef "health," with high coral cover and high ratios suggesting good "health," and low cover and low ratios suggesting poor "health."

By this metric, the two reefs nearest to Stone Town, which are those near the Chapwani and Bat Islands and Panga Island, are "unhealthiest," with low coral cover and low *Acropora*/*Porites* ratios, whereby the reef near Panga Island is the "healthier" of both. The reefs near Bawe, Nyange, and Chumbe Islands are the "healthiest," with high coral cover and high *Acropora*/*Porites* ratios, whereby the reef near Chumbe Island is the "healthiest" of all.

Another indicator of coral health is the degree of diversity within a coral reef, which was also analyzed. The observed diversity agree with a diversity study by *Zvuloni et al*. [2010], which concludes that the diversity near Stone Town and surrounding islands is low and increases toward Chumbe Island, i.e., more generally, diversity increases farther offshore and to the south from Stone Town.

Concentrations of total suspended solids (TSS) and chlorophyll-a at the surface were measured at locations on arcs centered at Stone Town on 5 and 2 days, respectively, in July and August 2011. In addition, chlorophyll-a concentrations were measured in the interior of the channel at locations on the transects in the austral winter of 2009 and 2011. All locations are indicated by crosses in Figure 3. TSS was sampled using the standard method described in *APHA, AWWA, and WEF* [2005]. To determine the chlorophyll-a concentration, the water samples were filtered, using Whatmann GF/F 25 mm filters, and stored at -17°C until they were analyzed. The samples were analyzed according to the procedures of *Aminot and Rey* [2000], using a UV-1601 Shimadzu spectrophotometer, and chlorophyll-a concentrations were calculated, using the trichromatic equations of *Jeffrey and Humphrey* [1975]. TSS is known to reduce irradiance to reef corals and chlorophyll-a is considered to be a reliable indicator of nutrient availability and water-column productivity [*Brodie et al*., 1997; *van Woesik et al*., 1999].

No significant spatial or temporal variations in TSS were found. The mean of all TSS samples was 11.62 μg/L with a standard deviation of 2.54 μg/L. For both days, that chlorophyll-a was measured on the arcs, concentrations of chlorophyll-a were significantly higher north than south of Stone Town. The mean chlorophyll-a concentration on the arcs was 0.33 μg/L with a standard deviation of 0.21 μg/L. This is comparable to the mean chlorophyll-a concentration on the transects in the interior of the channel of 0.34 μg/L with a standard deviation of 0.06 μg/L.

4. Description of the Dynamics

The strong agreement between the observed and modeled dynamics suggests that the ZCM may be used as a tool to investigate the dynamics of the Zanzibar Channel. In the following, some aspects of the dynamics of the ZCM are presented and additional observations are introduced for further comparison with the ZCM.

4.1. Velocity

On a seasonal scale, the dynamics of the Zanzibar Channel is dominated by two components. One is the remotely forced flow, which is predominantly the EACC, and the other the wind-forced flow in the surface Ekman layer.

The seasonally varying velocity field in the Zanzibar Channel is presented by both Figures 12 and 6 by showing the mean velocity field for four different 3-month periods of the year. Figure 12 shows the surface velocity field, while Figure 6 shows the vertical profile of the meridional velocity component. To aid in the description of the seasonally varying velocity field, the mean direction and magnitude of the wind measured by the Chukwani meteorological station is depicted by a thick black arrow in Figure 12.

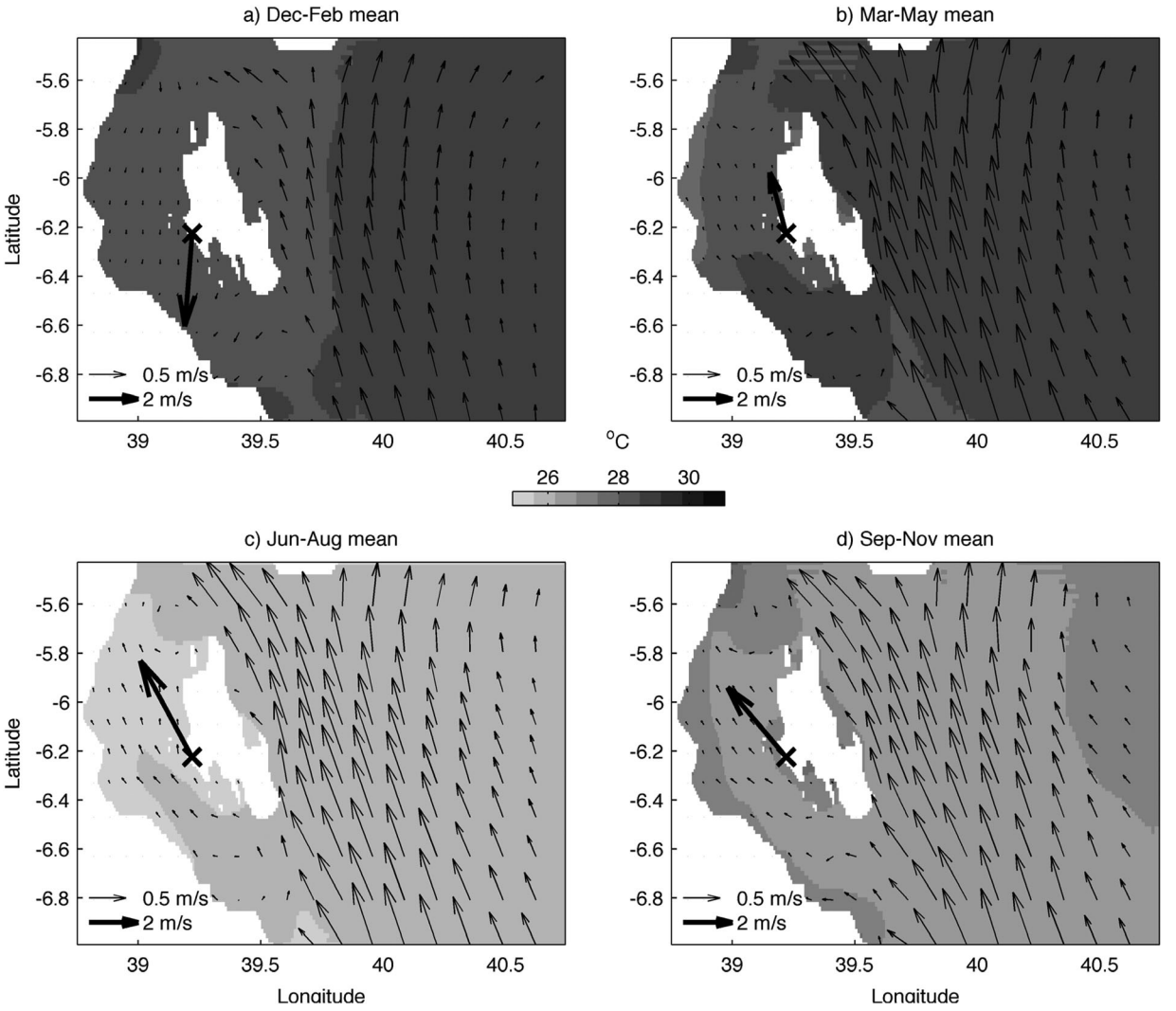

Figure 12. Seasonal cycles of the ZCM surface velocity field and SST. The mean surface velocity field (thin arrows) and the mean SST (contours) of the ZCM are shown for the periods December–February in Figure 12a, March–May in Figure 12b, June–August in Figure 12c, and September–November in Figure 12d. For clarity, the individual velocities are not shown at all ZCM grid points. The corresponding mean wind measured at the Chukwani meteorological station is shown by the thick arrow. The wind enhances the seasonality in the surface Ekman layer, as shown in Figure 6, and therefore the eastward shift of the surface flow during December–February apparent in Figure 12a does not imply an eastward shift of the EACC. The southern opening of the Pemba Channel is shown in the top left corner of each plot.

During the northeast monsoon season from December to February the wind is northerly, forcing a weak southward flow in the surface Ekman Layer inside the Zanzibar Channel, along the east coast of Zanzibar Island, and at the southern opening of the Pemba Channel located to the north of the Zanzibar Channel (arrows in Figure 12a and dashed line in Figure 6). Below the surface Ekman layer, the remotely forced flow component, which is primarily the EACC, is weakly northward (dashed line in Figure 6). Thus, during the northeast monsoon season, the wind-forced flow acts in the surface Ekman layer against the northward-flowing EACC. The surface velocity field shown by Figure 12a therefore gives the incorrect impression that the EACC shifts eastward and no longer flows through the Zanzibar and Pemba Channels. In reality, the EACC is not shifting during the northeast monsoon season, but instead continues to flow northward below the surface Ekman layer. This becomes evident when considering that the annual mean northward transport through the Pemba Channel is 5 Sv with a standard deviation of only 1 Sv. During the southwest monsoon season from April to November, the flow forced by the southeasterly wind acts in the surface Ekman layer in concert with the northward flowing EACC, resulting in a much stronger surface velocity field than during the northeast monsoon season (arrows in Figures 12b, 12c, and 12d and dotted, solid, and dashed-dotted lines in Figure 6). The wind-forced flow and the EACC both increase steadily until they both peak in

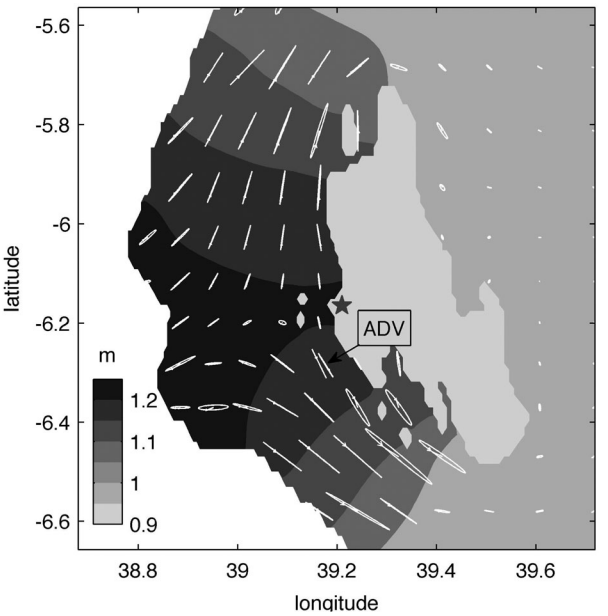

Figure 13. Tidal amplitude and ellipses. The M2 tidal constituent of the ZCM is presented by its sea level amplitude (contours) and tidal ellipses. The other five tidal constituents described by the ZCM have similar patterns. For clarity, the tidal ellipses are not shown at all ZCM grid points. The tidal ellipse obtained from measured velocity near Chumbe Island is also shown and labeled "ADV." The sea level amplitude and tidal ellipses visualize the cyclic pattern of the tidal flow, which is characterized by increasing and later decreasing flows directed into the channel at both openings until the accumulation of mass in the central channel reaches its maximum, followed by a reversal of this flow.

the austral winter months and then decrease again until the onset of the northeast monsoon season. Considering the dynamics during both monsoon seasons makes clear that the monsoon wind in the Zanzibar Channel enhances the seasonality of the dynamics in the surface Ekman layer.

The tidal dynamics of the Zanzibar Channel is dominated by the M2 tidal constituent, and therefore the M2 sea surface height amplitude and tidal ellipses are shown in Figure 13 to highlight the major features of the tidal dynamics. The tidal ellipse of the velocity measured by the ADV near Chumbe Island and described in section 3 is also depicted and presents another good agreement between observations and the ZCM. The patterns of the sea surface height amplitude and the tidal ellipses of the other five tidal constituents of the ZCM are similar and are therefore not shown.

The cyclic flow pattern of the tide cannot be completely understood from Figure 13 alone. Considering in addition the evolution of the tide described by the ZCM (not shown), reveals that at ebb tide at Stone Town (star in Figure 13), water begins to flow with increasing speed into the channel at both its northern and southern openings and to converge in the central channel. One quarter cycle later, which is 3 h for the dominant M2 tidal constituent, the speed of the flow at the channel opening has reached its maximum. At the end of a second quarter cycle, the accumulation of water in the central channel is maximal and the flow speed in the entire channel minimal. This marks the high tide at Stone Town. This flow pattern then reverses for two quarter cycles, resulting in ebb tide at Stone Town. The velocity ellipses shown in Figure 13 are consistent with this pattern. They are nearly one-dimensional and appear in the central channel to be aligned with the crest of the accumulated mass and away from the central channel aligned with the channel isobaths, indicating that the tidal flow follows isobaths as it flows back and forth between the respective channel openings and the central channel. *Shaghude et al*. [2002] suggest a similar tidal pattern based on short records of velocity measured by current meters north and south of Stone Town.

4.2. Transports

The seasonal variations of the modeled meridional transport in the Zanzibar Channel and in the upper 500 db east of Zanzibar Island are both shown by the thick gray and black lines in Figure 14, respectively. The scaling for each transport is chosen such that the ratio of the scales is identical to the ratio of the annual means of the transports. This implies that both annual means coincide in Figure 14. The modeled transport in the upper 500 db east of Zanzibar Island can be compared with an observed transport that has an annual mean of 27.3 Sv and a standard deviation of 2.6 Sv, which was obtained from several estimates of the transport in the upper 500 db east of Zanzibar Island between 4°S and 5°S obtained by *Swallow et al*. [1991] as part of a study of the structure and transport of the EACC, using historical hydrographic data binned by 1° latitude bands. The order of magnitude of the transport of the ZCM can be considered consistent with these estimates, especially by taking into account possible estimation errors and interannual variability of the actual transport.

The annual mean of the modeled transport in the channel is 0.029 Sv, which is less than 1% of the annual mean of the modeled transport in the upper 500 db east of Zanzibar Island. By estimating the total volume

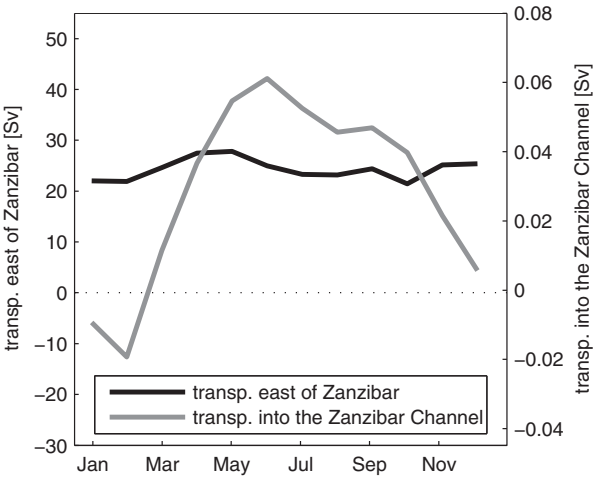

Figure 14. Seasonal cycles of the ZCM transport in the Zanzibar Channel and east of Zanzibar Island. The transport in the upper 500 db east of Zanzibar Island is shown by the thick black line and in the Zanzibar Channel by the thick gray line. The very different scales for showing the transports in the channel and east of Zanzibar Island were chosen such that the respective means coincide. The channel cross section is small compared to that of the open ocean, as evident in Figure 2b, and therefore the transport in the channel is less than 1% of the transport in the upper 500 db east of Zanzibar Island. However, the seasonal variation of the transport in the Zanzibar Channel is 9 times larger relative to its mean than that of the transport in the upper 500 db east of Zanzibar Island.

of the Zanzibar Channel to be approximately 10^{11} m^3, this annual mean transport implies a mean residence time for the water in the channel of 40 days. At the peak of the southwest monsoon season in June the monthly mean transport peaks at 0.061 Sv, implying a mean residence time of just 19 days.

The seasonal variation relative to its mean of the modeled transport in the channel is 9 times larger than east of Zanzibar Island, where the seasonal variation is taken to be the difference between the maximum and minimum of the respective transport. This is because the wind-forced flow enhances the seasonality and since the channel is shallow compared to the ocean east of Zanzibar Island, the contribution of the wind-forced flow relative to the total flow is much larger in the channel than east of Zanzibar Island.

The transport in the channel is composed of contributions by the remotely forced flow, which is predominantly the EACC, the wind-forced flow, and the tidal flow. To investigate the relative importance of these contributions, two modified versions of the ZCM were created, one without the wind forcing anywhere in the model domain, referred to as ZCM-no-wind, and one without the tidal forcing, referred to as ZCM-no-tide. Figure 15b shows the seasonal variations of the monthly means of the transports described by the ZCM and its two modified versions. For reference, Figure 15a shows the seasonal variation of the monthly mean wind measured by the Chukwani meteorological station.

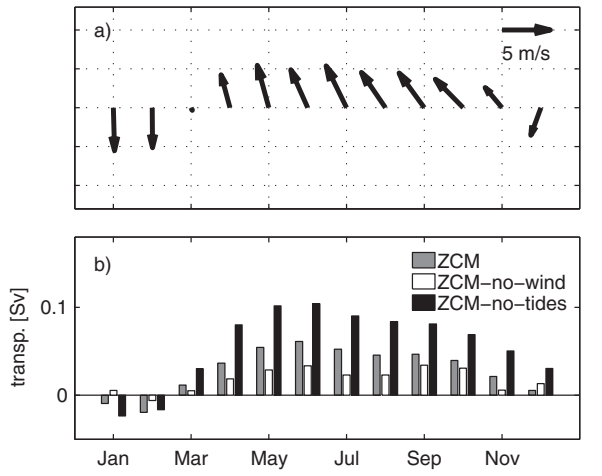

Figure 15. Seasonal cycles of the ZCM transport. The seasonal cycle of the monthly mean wind measured by the Chukwani meteorological station is shown in Figure 15a. The seasonal cycle of the monthly mean transport in the Zanzibar Channel is presented in Figure 15b. The gray bars show the ZCM transport, the white bars the ZCM-no-wind transport, which is the transport of the ZCM version without wind forcing, and the black bars the ZCM-no-tides, which is the transport of the ZCM version without tides. This shows that the wind increases the net transport, while the tide reduces it.

In the absence of wind, Figure 15 shows that the monthly mean transport is northward, except in February when it is southward (white bars). Comparing this to the transport described by the ZCM (gray bars) elucidates the effect of the wind. During the northeast monsoon season from December to February, the northerly wind reduces this northward transport in December and January and enhances the southward transport in February. During the southwest monsoon season from April to November, the southeasterly wind enhances the northward transport. The presence of the wind accounts for 0.011 Sv, which represents 38% of the annual mean of the total transport.

In the absence of tides, Figure 15 shows that the monthly mean transport increases, regardless of whether it is northward or southward, as seen by comparing the gray and black bars in

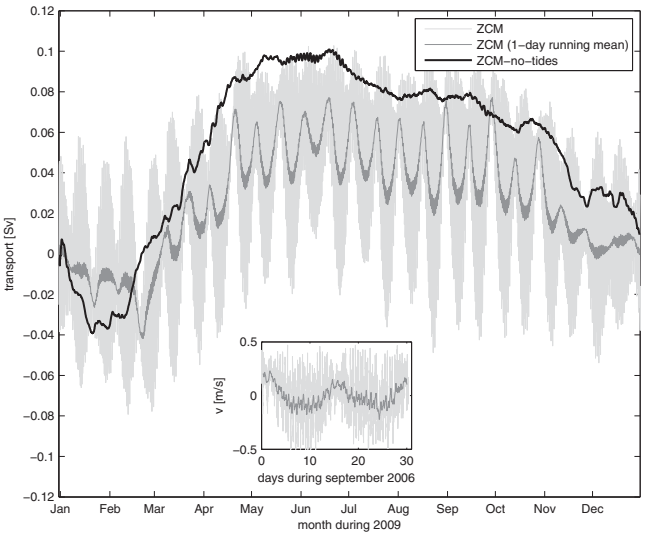

Figure 16. Transport. The 2 h ZCM transport in the Zanzibar Channel (light gray line) and its 1-day running mean (dark gray line) is shown. In addition, the 2 h ZCM-no-tides transport (black line), which is the transport of the ZCM version without tides, is shown. The inset shows the observed meridional velocity (light gray line) and its 1-day running mean (dark gray line) near Chumbe Island (northern black box in Figure 3c). The transports are shown at a higher temporal resolution than in Figure 15 and thus reveal that the net transport reduction by the tide oscillates with a period of 15 days. This oscillation coincides with the alternation between spring tide, characterized by largest variability in the 2 h ZCM transport (light gray line), and the neap tide, characterized by the smallest variability in the 2 h ZCM transport (light gray line).

Figure 15. The annual mean transport increases by 0.028 Sv, which represents 97% of the annual mean of the total transport. The tide can therefore be considered to reduce the transport regardless of its direction. Further details of this reduction are revealed by considering the transport not given every month, as in Figure 15, but every 2 h, as in Figure 16. It shows the transport of the ZCM (light gray line) and its 1-day running mean (dark gray line) as well as the transport of ZCM-no-tides (black line). The transport of the ZCM (light gray line) clearly shows the alternation between spring and neap tides, characterized by the alternation between high and low variability, respectively. Its 1-day running mean (dark gray line) helps to make it evident that the reduction of the transport oscillates with a period of about 15 days and that this oscillation coincides with the alternation between spring and neap tides. This means that during a spring tide the tidal flows are stronger and the reduction of the transport is at its maximum and during a neap tide the tidal flows are weaker and the reduction of the transport is at its minimum. In other words, the stronger the tidal flow, the stronger the reduction of the transport. This modeled phenomenon has been observed through velocity measurements made by an ADV for 1 month in September 2006 and are shown in the inset of Figure 16 (data provided by the Institute of Marine Sciences of the University of Dar es Salaam). The reason for the apparent relation between the tides and the reduction of the transport is not entirely clear. A thorough investigation into this relation would therefore require a series of detailed analyses which is beyond the scope of this paper.

4.3. Kinetic Energy Distribution

A measure of the relative importance of the components of the seasonal and tidal dynamics of the Zanzibar Channel can be taken to be their respective average kinetic energies. Each component can be represented by a vector $\mathbf{u}_x$, representing its depth-averaged horizontal velocity field. The seasonal dynamics is composed of the remotely forced flow, which is predominantly the EACC, denoted by $\mathbf{u}_r$, and of the wind-forced flow, denoted by $\mathbf{u}_w$. The tidal dynamics can be decomposed into the tidal flow as given by the six tidal constituents, denoted by $\mathbf{u}_{tc}$, and a tidal residual flow, denoted by $\mathbf{u}_{tr}$.

The average total kinetic energy is proportional to $\overline{\mathbf{u}\mathbf{u}}$, where $\mathbf{u}$ represents the depth-averaged horizontal velocity field of the total flow and the overbar represents the average over the area of the Zanzibar Channel circumscribed by the lines in the channel openings, shown in Figure 2, and the one year described by ZCM. Using the decomposition $\mathbf{u}=\mathbf{u}_r+\mathbf{u}_w+\mathbf{u}_{tc}+\mathbf{u}_{tr}$, gives,

$$\overline{\mathbf{u}\mathbf{u}}=\overline{\mathbf{u}_r\mathbf{u}_r}+\overline{\mathbf{u}_w\mathbf{u}_w}+\overline{\mathbf{u}_{tc}\mathbf{u}_{tc}}+\overline{\mathbf{u}_{tr}\mathbf{u}_{tr}}+\mathbf{r}, \tag{1}$$

where $\mathbf{r}=2(\overline{\mathbf{u}_r\mathbf{u}_w}+\overline{\mathbf{u}_r\mathbf{u}_{tc}}+\overline{\mathbf{u}_r\mathbf{u}_{tr}}+\overline{\mathbf{u}_w\mathbf{u}_{tc}}+\overline{\mathbf{u}_w\mathbf{u}_{tr}}+\overline{\mathbf{u}_{tc}\mathbf{u}_{tr}})$. The first four terms on the right-hand side of (1) are proportional to the four components' average kinetic energies, respectively. This requires the determination of the components $\mathbf{u}_r$, $\mathbf{u}_w$, $\mathbf{u}_{tc}$, and $\mathbf{u}_{tr}$. Harmonic analysis gives $\mathbf{u}_{tc}$. For ZCM-no-wind, the total flow is represented by $\mathbf{u}_{nw}=\mathbf{u}_r+\mathbf{u}_{tc}+\mathbf{u}_{tr}$. Subtracting $\mathbf{u}$ from $\mathbf{u}_{nw}$, gives $\mathbf{u}_w$. This leaves the two terms in the sum $\mathbf{u}_r+\mathbf{u}_{tr}$ to be separated. Because the boundary forcing is purely seasonal, $\mathbf{u}_r$ is consequently also purely seasonal, while $\mathbf{u}_{tr}$ does not have a seasonally varying component. This makes the separation possible, which is

achieved by defining $\mathbf{u}_r$ to be equal to the first two harmonics of the annual cycle fitted to $\mathbf{u}_r + \mathbf{u}_{tr}$. This is an appropriate definition because those two harmonics capture the seasonal cycle most accurately [e.g., *Yashayaev and Zveraev*, 2001]. The average kinetic energies of the remotely forced flow, wind-forced flow, six tidal constituents, and residual tidal flow relative to the average total kinetic energy can thus be calculated and are 5%, 3%, 91%, and 1%, respectively, while much less than 1% are represented by **r**.

This distribution of the kinetic energy indicates that the dynamics of the Zanzibar Channel is almost entirely tidal. This, however, does not mean that the other two components can be generally neglected. The tidal dynamics is highly oscillatory, and therefore the other two components, whose flow is relatively more steady, become important, e.g., in considering the advection of polluted water in the channel out to the open ocean.

4.4. Temperature

The Zanzibar Channel is well mixed, except for two brief periods described in the next section, and thus the SST is representative of the temperature of the full water column. The spatial pattern of the ZCM SST for four 3-month periods of the year is shown in Figure 12, while its temporal evolution is shown in Figure 8a. During the northeast monsoon season from December to February, the wind is northerly and the high air temperature leads to relatively high SST in the region, except in the channel, which experiences a temporal cooling. This cooling could be caused by upwelling of deep cold water in the deep areas of the coastal ocean north of the Zanzibar Channel, caused by the prevailing northerly wind, followed by its advection into the Zanzibar Channel. In March, the wind reverses with its magnitude still small, and the air temperature reaches its maximum, allowing SST to reach also its maximum at around 29–30°C [*Mahongo and Shaghude*, 2014]. April marks the onset of the southwest monsoon season and SST begins to decrease gradually to about 25°C with the increasing southeasterly wind. Both reaching their respective minimum and maximum during the period from June to August. This gradual decrease of SST is mainly caused by the EACC outside the ZCM domain, which advects into the channel colder waters from an Ekman divergence zone in which cold subsurface waters are upwelled from the South Equatorial Current east of the northern tip of Madagascar [*Schott et al.*, 2009]. As the southeasterly wind decreases in magnitude from September to November, the SST gradually increases. December then marks the onset of the northeast monsoon season.

The temperature varies on a range of time scales. The temperature measured by the thermistors, shown by gray solid lines in Figure 10, exhibits, besides its seasonal variability, some variability on time scales of hours and days. Since the ZCM was developed to describe the seasonal and tidal dynamics, it is unable to describe the variations on the time scale of days. However, the ZCM does produce the variations on the time scale of hours (not shown) and it was found that these variations have a semidiurnal frequency, clearly associated with the tide. The ZCM suggests that the tide advects horizontal temperature gradients across the location of the thermistors, thus creating the variations in temperature. These variations are stronger at the southern location, where thermistors were deployed close to the entrance of a bay (southern triangle in Figure 3). The reason for the variations being stronger is that the bay is typically warmer than the surrounding waters, which enhances the horizontal temperature gradient.

4.5. Stratification

The Zanzibar Channel is well mixed for most of the year. The daily warming of the surface during daytime does create a stratification, but it is hardly recognizable and disappears again during nighttime. The only notable stratification occurs briefly and is due to freshwater influx at the surface from heavy rains from March to May and moderate rains from November to December. These two rainy seasons are, respectively, associated with the northward and southward movement of the Inter-Tropical Convergence Zone (ITCZ) [*Mahongo and Francis*, 2012].

Figure 17 shows the stratification at a location in the middle of the Zanzibar Channel, marked by a star in Figure 2a. The stratification is defined for the present purpose as the density at the bottom minus the density at the surface, where the density difference purely due to the temperature difference and purely due to the salinity difference is shown separately, using the linearized equation of state. In this way, the relative contributions of the temperature and salinity differences to the density difference, and thus the stratification, is elucidated. During the time periods with heavy rains the maximum total density difference is 0.18

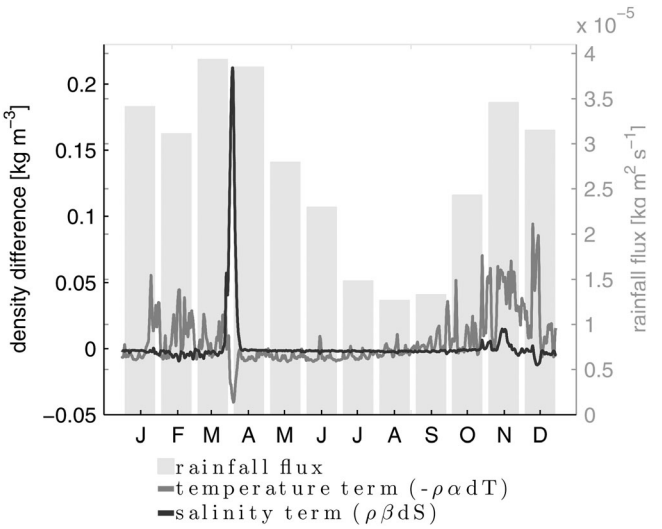

Figure 17. ZCM stratification and rainfall. The stratification in the center of the Zanzibar Channel (star in Figure 2) is shown as the density at the bottom minus the density at the surface, whereby the contribution to this density difference due to the salinity difference and temperature difference, as determined by the linearized equation of state, is shown separately by the black and dark gray lines, respectively. The rainfall flux is shown by the light gray bars. The channel is well mixed, except during brief periods in the two rainy seasons.

kg/m^3 with −0.04 kg/m^3 caused by a temperature difference of 0.17°C and 0.22 kg/m^3 caused by a salinity difference of 0.30. During the time periods with moderate rains the corresponding values are 0.07 kg/m^3, 0.06 kg/m^3, −0.52°C, 0.01 kg/m^3, and 0.03.

During the time period with heavy rains, the salinity difference of 0.3 briefly emerges before it is eliminated by mixing. As a result, the salinity in the channel drops, but by 0.7 from 35.7 to 35.0, which is a larger drop than can be explained in terms of the heavy rains alone. A feasible hypothesis is that fresher water due to rains outside the ZCM domain are advected into the channel by the remotely forced flow, which is predominately the EACC.

5. Application Example

The ZCM can be applied to help address issues of interest to marine resource management. These issues are, for instance, the dispersion of sewage pollution or coral larvae, which are of ecological and socioeconomic importance. Dispersion of sewage pollution in the channel is becoming a growing problem that can affect human health [*Mohammed*, 2002; *Moynihan et al*., 2012] and biodiversity [*Harvell et al*., 2004], especially because sewage pollution is considered the most important local factor affecting coral reefs worldwide [*Halpern et al*., 2008]. Dispersion of coral larvae is important because it represents the connectivity between coral reefs that is crucial for their survival. Besides those two concrete cases, dispersion studies might also be able to help explain the poorly understood spatial distribution of seagrass and thus its current decline [*Knudby and Nordlund*, 2011]. This is a problem not only in the channel, but beyond it in several coastal areas of the western Indian Ocean, and it affects local populations as they depend on invertebrates found in seagrass beds [*Gössling et al*., 2004].

As a simple application example, passive tracers, which approximate sewage pollution, are released at two grid points in the ZCM only at the start of the model simulation, where the single grid points are indicated by crosses in Figure 18. A more realistic application that would have continuous sources of passive tracers at multiple locations in the channel is beyond the objective of presenting a simple application example. One of the two grid points at which passive tracers were released in the ZCM is located at Shangani, which is one of five main sources of sewage pollution in the Stone Town area, as identified by *Moynihan et al*. [2012]. The other four are all within a few grid points of the grid point at which passive tracers were released in the ZCM. The release of passive tracers at this one grid point is therefore intended to be representative all five main sources of sewage pollution in the Stone Town area. The other grid point at which passive tracers were released in the ZCM is located at Dar es Salaam, the capital and largest city of Tanzania. To show the dispersion of the released passive tracers during both the southwest and northeast monsoon seasons, the ZCM was integrated twice for the duration of 1 month, once initialized with its 1 June and 1 January states, respectively.

Figure 18 shows the time evolution of the passive tracers' surface concentration relative to their concentrations at the single grid points where they were released at the start of the simulations for both the southwest and northeast monsoon seasons in the top and bottom plots, respectively. The passive tracers' concentrations below 1% are not shown. Because the passive tracers are generally advected away from their sources, it is possible to show in each plot the passive tracers' surface concentration after 1, 5, and 10 days of the start of the simulations in the form of three distinguishable contoured patches at an increasing

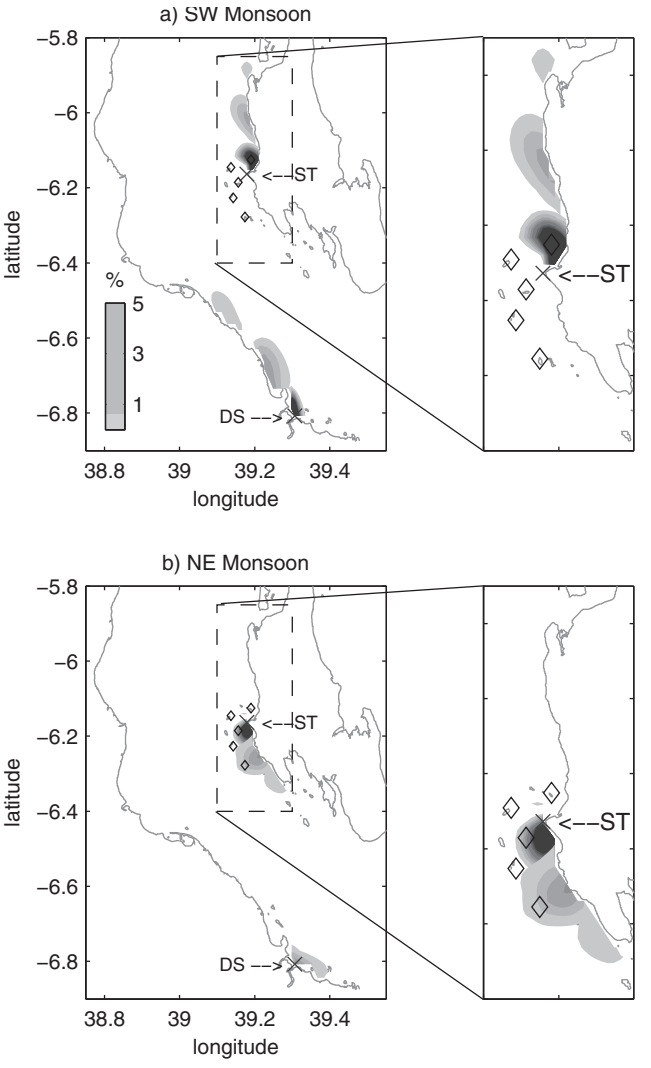

Figure 18. Dispersion of passive tracers in the ZCM. Passive tracers with a concentration of 100% were released in the ZCM near Stone Town (ST) and Dar es Salaam (DS) during the southwest monsoon season presented in Figure 18a and the northeast monsoon season presented in Figure 18b. Since the passive tracers move steadily away from their sources their concentrations are plotted by distinguishable contoured patches 1, 5, and 10 days after they were released. The only exception are the passive tracers released at Dar es Salaam during the northeast monsoon season because they do not move and therefore only their concentration after 10 days is plotted by one contoured patch. Except for this one case, the passive tracers disperse along and close to the coast. The diamonds indicate the five sites near small islands where photographs of coral reefs were taken. These islands are, listed from north to south: Chapwani and Bat, Bawe, Pange, Nyange, and Chumbe.

distance from the passive tracers' sources. It is apparent that the passive tracers are advected by the velocity field and diluted in the process. The only exception are the passive tracers at Dar es Salaam during the northeast monsoon season because they are not advected, but still diluted similarly to the passive tracers during the southwest monsoon. Since therefore the passive tracers' surface concentrations cannot be shown for all 3 times for this one case, they are only shown after 10 days.

In all cases, except one, the passive tracers are advected along and close to the coast, which means that they remain in shallow areas, where coral reefs and seagrass beds are typically found. Furthermore, the southwest monsoon season lasts much longer than the northeast monsoon season. Both facts combined implies that continuous sewage entering the channel at Stone Town and at Dar es Salaam would cause pollution all along and close to the coast, while the sewage pollution north of its entry point would be greater than south of it.

The observed status of coral reefs and chlorophyll-a concentrations, presented in section 3, is consistent with the predictions of the dispersion of sewage pollution from a source at Stone Town. Coral assemblages clearly reflect the long-term chemical and physical conditions of their environment. They thus also reflect the presence of sewage pollution in their environment, which has the capacity to disrupt coral-dinoflagellates symbiosis and cause mortality of sensitive corals, such as *Acropora*. The quality of coral reefs is therefore ideal to compare with the dispersion of sewage pollution. Using both simulations and the relative duration of both monsoon seasons, make it possible to estimate the cumulative sewage pollution at every grid point. A generalized additive model shows a significant inverse relationship between this cumulative sewage pollution estimate and the percentage coral cover across all sites. High percentage coral cover is observed where the simulations predict low pollutant concentrations and vice versa. In addition, the ratio of *Acropora*/*Porites* across all sites is consistent with this finding. Further support of the model predictions is provided by the observed chlorophyll-a concentrations, which are higher north than south of Stone Town. However, sewage does not only contain nutrients, which among other effects promote the growth of chlorophyll-a, but a plethora of toxins potentially damaging to coral reefs.

This simple application example could be used to test hypotheses that could motivate changes in sewage disposal practices. For example, the model could be used to simulate the dispersion of sewage pollution that is pumped through a pipe from Stone Town and released offshore. The sewage pollution might be dispersed away from the coastline, causing less damage to coastal reefs than the present sewage pollution from the source at Stone Town.

Björk et al. [1995] argues that the tide causes the considerable spatial and temporal variance of pollution and that pollutants are flushed from the coast and dispersed within one tidal cycle. It is certainly true that the tide supports the dispersion of pollutants, but the tide is oscillatory. More so than the tide, it is the remotely forced flow, which is predominantly the EACC, and the wind-forced flow that transport the pollution away from Stone Town and most likely out of the Zanzibar Channel. The time it takes to flush the pollution out of the Zanzibar Channel is estimated in section 4.2 and can be as short as 19 days, which is, however, still much longer than a tidal cycle.

This application of the ZCM highlights that interactions of physical and biological processes are important. For other coastal oceans, models of complex biophysical interactions have already been proven to be beneficial to scientists and marine resource managers [e.g., *Pfeiffer-Herbert et al*., 2007; *Fiechter et al*., 2011; *Auad and Martos*, 2012; *Ibarra et al*., 2014].

6. Conclusion

The seasonal and tidal dynamics of the Zanzibar Channel described by the ZCM compares well with observations, and thus represents an effective tool to investigate the dynamics and to develop applications that address important ecological and socioeconomic issues in the Zanzibar Channel region.

The ZCM shows that the seasonal dynamics in the Zanzibar Channel is forced remotely, which creates primarily the EACC in the Zanzibar Channel region, and by the local, mainly monsoonal wind, which forces a flow in the surface Ekman Layer. During the northeast monsoon season from December to February, the flow in the surface Ekman layer acts against, and thereby weakens, the northward-flowing EACC, while during the southwest monsoon season from March to November, it strengthens the northward-flowing EACC. The wind thus enhances the seasonality in the surface Ekman layer.

The tidal dynamics varies on a semidiurnal scale since the M2 tidal constituent is the most dominant in the Zanzibar Channel. It follows a pattern in which water flows into the channel through both openings and accumulates in the central channel. High tide occurs when this accumulation of water reaches its maximum. This flow then reverses and ebb tide occurs when a maximum amount of water has left the channel.

Although the seasonal and tidal dynamics appear to be distinctly different they are intimately connected. In the presence of the tide, the transport is reduced regardless of its direction. This reduction varies with a period of about 15 days and appears to be related to the tide because the reduction is strongest during spring tide and weakest during neap tide. The reason for this apparent relation is not entirely clear and requires further investigations.

To obtain an understanding of the relative importance of the different flow components in some aspects is to determine the average kinetic energy each of them contains. By far the most kinetic energy is contained by the tide with 91% and 1% of the total average kinetic energy contained in the tidal flow representing the tidal constituents imposed on the ZCM and in the tidal residual flow, respectively. The remotely forced flow contains 5% and the wind-forced flow 3%. While the tide contains most of the kinetic energy, the remotely forced and wind-forced flows are more effective in the advection of water over longer times and distances, which is important for the dispersion of passive tracers such as sewage pollution and coral larvae.

The Zanzibar Channel is usually well mixed, except during the two rainy seasons from March to May and from November to December. The temperature of the channel has a typical seasonal variation with low temperatures during the austral winter and high temperatures during the austral summer, except for a temporal cooling from December to February. The cause of this temporal cooling could be the northerly monsoon wind, which may force upwelling of cold water in the deep coastal ocean north of the Zanzibar Channel, and subsequently this cold water is advected into the channel. The time of the onset of the temporal cooling as well as its exact evolution appears to vary significantly from year to year.

This paper does not present the complete dynamics of the Zanzibar Channel, which raises several questions. For instance, what would the dynamics of the subseasonal scale look like? Would the dynamics on this subseasonal scale substantially interact with the dynamics on other scales? These questions have not been addressed previously and their answers remain as speculation. An analysis of measured wind provided by NOAA's National Climate Data Center (NOAA-NCDC) from the Chukwani meteorological station as well as from stations in Dar es Salaam and Mombasa, Kenya reveals that almost the same amount of kinetic energy that is contained in the seasonal wind is contained in the subseasonal wind, which is for the present purposes defined to be the daily anomaly from the respective seasonal cycle. However, the seasonal wind is highly anisotropic and long-lived due to the two prevalent wind directions during the two monsoon seasons, while the subseasonal wind is highly isotropic and short-lived. A modified version of the ZCM with the seasonal wind replaced by 3 hourly wind indicates that the subseasonal dynamics in the Zanzibar Channel is, as the subseasonal wind, highly isotropic. Because of its isotropy, the subseasonal dynamics makes a negligibly small contribution to the transport in the channel. In other respects, too, the subseasonal dynamics is expected to have little effect on the seasonal dynamics. This expectation is based on the finding that the seasonal dynamics of the ZCM, which contains no subseasonal dynamics, compares well with observations of the seasonal dynamics of the Zanzibar Channel, which contains dynamics on other scales. The subseasonal dynamics, as the subseasonal wind, most likely also contains a notable amount of kinetic energy. An indication that this might be the case is given by the measured temperature presented by Figure 10, which shows that the variability on scales of several days, hence subseasonal, during some time periods of the year is not negligible compared to the seasonal variability.

The ZCM has many potential applications. One, highlighted in this paper, is the study of the dispersion of passive tracers, such as sewage pollution. Despite its simplicity, it predicts that sewage pollution emanating from Stone Town and Dar es Salaam disperses along and close to the respective coasts with more sewage pollution dispersing toward the north than the south. The available observations around Stone Town are consistent with this prediction. A refined version of this application could already be a decision support tool that would help better manage the pollution of the Zanzibar Channel. Another application of the ZCM could be its integration with a biological model that would allow connectivity studies, which are efforts to understand how coral larvae drift between different coral reefs, which is a crucial factor in the coral reefs' survival. Such a combination of models could therefore become decision support tools in the effort to protect and manage the Zanzibar Channel's marine life. As a third example, an application could be developed based on the fact that the ZCM can precisely predict the tidal dynamics and since the tidal dynamics contains 91% of the average total kinetic energy, the prediction of the tidal dynamics alone, given by harmonic analysis, could be sufficient to provide useful forecasts for navigation and guidance for observational studies. Lastly, the ZCM domain was chosen large enough in order for the ZCM to be forced by the output of OGCMs. This creates the possibility to downscale climate projections by these OGCMs to the regional scale.

Acknowledgments

The data that was used for the results of this paper can be made available upon request from the corresponding author (jzavala@marine.rutgers.edu). This paper is based upon work supported by the National Science Foundation primarily under grant OISE-0827059 and partially also under grants OCE-0550658, OCE-0851493, and OCE-0927472. Further support was provided by The Cornell Commitment and The DotGreen Foundation. The authors are immensely grateful to the various and invaluable contributions from Chloe Anderson; Brian Arbic; Christopher Cacciapaglia; Chumbe Island Coral Park, especially Kina Mtwana-Nordlund; Emanuele Di Lorenzo; Alfonse Dubi; Julius Francis; Sharon Franks; Ralf Goericke; Heath Hansell; Anthony Hooten; the Institute of Marine Sciences of the University of Dar es Salam, especially Narriman Jiddawi, Margaret Kyewalyanga, Juma Kifana Makame, Aviti Mmochi, Christopher Muhando, Ntahondi Nyandwi, and Edna Nyika; the Intergovernmental Oceanographic Commission at UNESCO, especially Joannes Berque, Ehrlich Desa, and Stefano Mazzilli; JAMSTEC, especially Hide Sasaki; Andrew Kough; Shigalla Mahongo; Matt Moldovan; Samiah Moustafa; Patrick Nadeau; Nakupenda Safaris, especially Khamis Khamis; Mohammed Ngwali; Aurelien Ponte; Carly Randall; Chris Reason; Travis Schramek; Andrey Shcherbina; Teledyne RD Instruments, especially Patrick Bradley, Dan Murphy, and Daniel Pedraza; Martin Theiss; Robert Thombley; Samuel Wilson; Clint Winant; Katherin Zaba; and Luis Zamudio.

References

Aminot, A., and F. Rey (2000), Standard procedures for the determination of chlorophyll a by spectroscopic methods, in *International Council for the Exploration of the Sea*, pp. 7–10, Copenhagen, Denmark.

APHA, AWWA, and WEF (2005), *Standard Methods for the Examination of Water and Wastewater*, edited by M. A. H. Franson, American Public Health Association, Washington, D. C.

Auad, G., and P. Martos (2012), Climate variability of the Northern Argentinean shelf circulation: Impact on Engraulis Anchoita, *Int. J. Ocean Clim. Syst.*, *3*(1), 17–43.

Björk, M., S. Mohammed, M. Björklund, and A. Semesi (1995), Coralline algae, important coral reef builders threatened by pollution, *Ambio*, *24*, 502–505.

Bleck, R. (2002), An oceanic general circulation model framed in hybrid isopycnic Cartesian coordinates, *Ocean Modell.*, *5*, 55–88.

Brodie, J., M. Furnas, A. Stevens, L. Trott, F. Pantus, and M. Wright (1997), Monitoring chlorophyll in the great barrier reef lagoon: Trends and variability, in *Proceedings of the 8th International Coral Reef Symposium*, edited by H. A. Lessios and I. G. Macintyre, vol. 1, pp. 797–802, Smithson. Trop. Res. Inst., Panama.

Bryan, W. R., and F. O. Holland (1989), A high resolution simulation of the wind- and thermohaline-driven circulation in the North Atlantic Ocean, in *Parameterization of Small Scale Processes: Aha Huliko'a Hawaiian Winter Workshop*, edited by P. Müller and D. Henderson, Hawaii Inst. of Geophys, Honolulu.

Chapman, D. C. (1985), Numerical treatment of cross-shelf open boundaries in a barotropic coastal ocean model, *J. Phys. Oceanogr.*, *15*(8), 1060–1075.

Egbert, G. D., A. F. Bennett, and M. G. G. Foreman (1994), TOPEX/POSEIDON tides estimated using a global inverse model, *J. Geophys. Res.*, *99*(C12), 24,821–24,852.

Fairall, C., E. Bradley, J. Hare, A. Grachev, and J. Edson (2003), Bulk parameterization of air-sea fluxes: Updates and verification for the COARE algorithm, *J. Clim.*, *16*, 571–591.

Fiechter, J., G. Broquet, A. M. Moore, and H. G. Arango (2011), A data assimilative, coupled physical-biological model for the Coastal Gulf of Alaska, *Dyn. Atmos. Oceans*, *52*, 95–118.
Flather, R. A. (1976), A tidal model of the northwest European continental shelf, *Mem. Soc. R. Sci. Liege*, *6*(10), 141–164.
Golbuu, Y., R. van Woesik, R. Richmond, P. Harrison, and K. Fabricius (2011), River discharge reduces coral diversity in Palau, *Mar. Pollut. Bull.*, *62*, 824–831.
Gössling, S., T. Kunkel, K. Schumacher, and M. Zilger (2004), Use of molluscs, fish, and other marine taxa by tourism in Zanzibar, Tanzania, *Biodiversity Conserv.*, *13*, 2623–2639.
Haidvogel, D., H. Arango, K. Hedstrom, A. Beckmann, P. Malanotte-Rizzoli, and A. F. Shchepetkin (2000), Model evaluation experiments in the North Atlantic basin: Simulations in nonlinear terrain-following coordinates, *Dyn. Atmos. Oceans*, *32*(3–4), 239–281.
Haidvogel, D., et al. (2008), Ocean forecasting in terrain-following coordinates: Formulation and skill assessment of the Regional Ocean Modeling system, *J. Comput. Phys.*, *227*(7), 3595–3624.
Halpern, B., et al. (2008), A global map of human impact on marine ecosystems, *Science*, *319*(5865), 948–952.
Harvell, C. D., et al. (2004), The rising tide of ocean diseases: Unsolved problems and research priorities, *Front. Ecol. Environ.*, *2*(7), 375–382.
Hellerman, S., and M. Rosenstein (1983), Normal wind stress over the world ocean with error estimates, *J. Phys. Oceanogr.*, *13*, 1093–1104.
Ibarra, D. A., K. Fennel, and J. J. Cullen (2014), Coupling 3-d Eulerian bio-physics (ROMS) with individual-based shellfish ecophysiology (SHELL-E): A hybrid model for carrying capacity and environmental impacts of bivalve aquaculture, *Ecol. Modell.*, *273*, 63–78.
IOC (2009), Annual Report 2009, edited by T. Gross, IOC Annual Reports Series No. 16, UNESCO.
IOC (2012), Global sea level observing system (gloss) implementation plan—2012, *IOC Tech. Ser. 100*, Intergov. Oceanogr. Comm., Paris.
Jeffrey, S., and G. Humphrey (1975), New spectrophotometric equations for determining chlorophylls a, b, c1 and c2 in higher plants, algae and natural phytoplankton, *Biochem. Physiol. Pflanz.*, *167*, 191–194.
Jerlov, N. G. (1968), *Optical Oceanography*, Elsevier, N. Y.
Jones, W., and B. Launder (1972), The prediction of laminarization with a two-equation model of turbulence, *Int. J. Heat Mass Transfer*, *15*, 301–314.
Killworth, P. D. (1996), Time interpolation of forcing fields in ocean models, *J. Phys. Oceanogr.*, *26*, 136–143.
Knudby, A., and L. Nordlund (2011), Remote sensing of seagrasses in a patchy multi-species environment, *Int. J. Remote Sens.*, *32*(8), 2227–2244.
Kohler, K., and S. Gill (2006), Coral Point Count with Excel extensions (CPCe): A Visual Basic program for the determination of coral and substrate coverage using random point count methodology, *Comput. Geosci.*, *32*(9), 1259–1269.
Launder, B., and B. Sharma (1974), Application of the energy dissipation model of turbulence to the calculation of flow near a spinning disc, *Lett. Heat Mass Transfer*, *1*(2), 131–138.
Mahongo, S. B., and J. Francis (2010), Monthly variations in sea level at the island of Zanzibar, *Western Indian Ocean J. Mar. Sci.*, *9*, 1–16.
Mahongo, S. B., and J. Francis (2012), Analysis of Rainfall Variations and Trends in Coastal Tanzania, *Western Indian Ocean J. Mar. Sci.*, *11*(2), 121–133.
Mahongo, S. B., and Y. Shaghude (2014), Modelling the dynamics of the Tanzanian coastal waters, *J. Oceanogr. Mar. Sci.*, *5*, 1–7.
Mahongo, S. B., J. Francis, and S. E. Osima (2011), Wind patterns of coastal Tanzania: Their variability and trends, *Western Indian Ocean J. Mar. Sci.*, *10*(2), 107–120.
Marchesiello, P., J. C. McWilliams, and A. F. Shchepetkin (2001), Open boundary conditions for long-term integration of regional oceanic models, *Ocean Modell.*, *3*, 1–20.
Masumoto, Y., et al. (2004), A fifty-year eddy-resolving simulation of the world ocean—Preliminary outcomes of OFES (OGCM for the earth simulator), *J. Earth Simulator*, *1*, 35–56.
Mohammed, S. (2002), Pollution management in Zanzibar: The need for a new approach, *Ocean Coastal Manage.*, *45*, 301–311.
Moynihan, M., D. Baker, and A. Mmochi (2012), Isotopic and microbial indicators of sewage pollution from Stone Town, Zanzibar, Tanzania, *Mar. Pollut. Bull.*, *64*, 1348–1355.
Muhando, C. (2002), *Seawater temperature on shallow reefs off Zanzibar Town, Tanzania, in* Coral Degradation in the Indian Ocean: Status Report 2002, edited by O. Lindén et al., pp. 40–46, CORDIO, Dep. of Biol. and Environ. Sci., Univ. of Kalmar, Kalmar, Sweden.
Muzuka, A., A. Dubi, C. Muhando, and Y. Shaghude (2010), Impact of hydrographic parameters and seasonal variation in sediment fluxes on coral status at Chumbe and Bawe reefs, Zanzibar, Tanzania, *Estuarine Coastal Shelf Sci.*, *89*, 137–144.
Newell, B. (1957), A preliminary survey of the hydrography of the British East Africa Coastal waters, *Col. Off. Fish. Publ. 9*, London, U. K.
Ngusaru, A., and S. Mohammed (2002), Water, salt and stoichiometrically linked nutrient budgets for Chwaka Bay, Tanzania, *Western Indian Ocean J. Mar. Sci.*, *1*(2), 97–106.
Odido, M., and S. Mazzilli (Eds.) (2009), *African Oceans and Coasts, IOC Inform. Doc. 1255*, UNESCO Reg. Bur. for Sci. and Technol. in Africa, Kenya.
Paulson, C. A., and J. J. Simpson (1977), Irradiance measurements in the upper ocean, *J. Phys. Oceanogr.*, *7*, 952–956.
Pfeiffer-Herbert, A. S., M. A. McManus, P. T. Raimondi, Y. Chao, and F. Chai (2007), Dispersal of Barnacle larvae along the Central California Coast: A modeling study, *Limnol. Oceanogr.*, *52*(4), 1559–1569.
Rodi, W. (1984), *Turbulence models and their application in hydraulics: A state of the art review*, Int. Assoc. for Hydraul. Res., Delft, Netherlands.
Saha, S., et al. (2010), The NCEP climate forecast system reanalysis, *Bull. Am. Meteorol. Soc.*, *91*, 1015–1057.
Salon, S., A. Crise, and A. J. Van Loon (2011), Dynamics of the bottom boundary layer, in *Developments in Sedimentology*, vol. 60, edited by H. Hüneke and T. Mulder, chap. 6, pp. 83–97, Elsevier, Amsterdam.
Sasaki, H., M. Nonaka, Y. Masumoto, Y. Sasai, H. Uehara, and H. Sakuma (2008), An Eddy-Resolving Hindcast Simulation Of The Quasi-Global Ocean From 1950 to 2003 on the Earth Simulator, in *High Resolution Numerical Modelling of the Atmosphere and Ocean*, edited by K. Hamilton and W. Ohfuchi, chap. 10, pp. 157–186, Springer, N. Y.
Schott, F. A., S.-P. Xie, and J. P. McCreary Jr. (2009), Indian ocean circulation and climate variability, *Rev. Geophys.*, *47*, RG1002, doi:10.1029/2007RG000245.
Selig, E., K. Casey, and J. Bruno (2010), New insights into global patterns of ocean temperature anomalies: Implications for coral reef health and management, *Global Ecol. Biogeogr.*, *19*(3), 397–411.
Shaghude, Y., and K. Wannäs (1998), Morphology and sediment distribution of the Zanzibar Channel, *Ambio*, *27*, 729–733.
Shaghude, Y., and K. Wannäs (2000), Mineralogical and Biogenic Composition of the Zanzibar Channel Sediments, Tanzania, *Estuarine Coastal Shelf Sci.*, *51*, 477–489.
Shaghude, Y., K. Wannäs, and S. Mahongo (2002), Biogenic assemblage and hydrodynamic settings of the tidally dominated reef platform sediments of the Zanzibar Channel, *Western Indian Ocean J. Mar. Sci.*, *1*, 107–116.

Shchepetkin, A., and J. McWilliams (2003), A method for computing horizontal pressure-gradient force in an oceanic model with a non-aligned vertical coordinate, *J. Geophys. Res.*, *108*(C3), 3090, doi:10.1029/2001JC001047.

Shchepetkin, A., and J. C. McWilliams (2005), The Regional Ocean Modeling System (ROMS): A split-explicit, free-surface, topography-following coordinates ocean model, *Ocean Modell.*, *9*(4), 347–404.

Shchepetkin, A. F., and J. C. McWilliams (2009), Correction and commentary for Ocean forecasting in terrain-following coordinates: Formulation and skill assessment of the regional ocean modeling system by Haidvogel et al., J. Comp. Phys. 227, pp. 3595–3624, *J. Comp. Phys.*, *228*, 8985–9000.

Shetye, S., and A. Gouveia (1998), *Coastal circulation in the North Indian Ocean, in* The Sea*, vol. 11*, edited by A. Robinson and K. Brink, pp. 523–556, John Wiley, N. Y.

Swallow, J., F. Schott, and M. Fieux (1991), Structure and transport of the East African Coastal Current, *J. Geophys. Res.*, *96*(C12), 22,245–22,257.

United Nations (2002), Report of the world summit on sustainable development, *A/CONF.199/20*, N. Y.

van Woesik, R., T. Tomascik, and S. Blake (1999), Coral assemblages and physico-chemical characteristics of the Whitsunday Islands: Evidence of recent community changes, *Mar. Freshwater Res.*, *50*(5), 427–440.

van Woesik, R., J. Gilner, and A. J. Hooten (2009), Standard operating procedures for repeated measures of process and state variables of coral reef environments, in *Coral Reef Targeted Research and Capacity Building for Management Program*, Univ. of Queensland, St. Lucia. [Available at http://gefcoral.org/Portals/53/downloads/tools/CRTR%20-%20CS%20lres%20web%20reissue.pdf.]

Warner, J. C., C. R. Sherwood, H. G. Arango, and R. P. Signell (2005), Performance of four turbulence closure models implemented using a generic length scale method, *Ocean Modell.*, *8*, 81–113.

Warner, J. C., C. R. Sherwood, R. P. Signell, C. K. Harris, and H. G. Arango (2008), Development of a three-dimensional, regional, coupled wave, current, and sediment-transport model, *Comput. Geosci.*, *34*(10), 1284–1306.

Yashayaev, I. M., and I. I. Zveraev (2001), Climate of the seasonal cycle in the North Pacific and the North Atlantic Oceans, *Int. J. Climatol.*, *21*, 401–417.

Zvuloni, A., R. van Woesik, and Y. Loya (2010), Diversity partitioning of stony corals across multiple spatial scales around Zanzibar Island, Tanzania, *PLoS One*, *5*(3), e9941.